FINAL REPORT ~ FHWA-OK-15-05

EXPECTED LIFE OF SILANE WATER REPELLENT TREATMENTS ON BRIDGE DECKS PHASE 2

M. Tyler Ley, Ph.D., P.E.

Mehdi Khanzadeh Moradllo, Ph.D. Candidate

School of Civil and Environmental Engineering

College of Engineering, Architecture and Technology

Oklahoma State University

Stillwater, Oklahoma

October 2015

Oklahoma Department of Transportation

EXPECTED LIFE OF SILANE WATER REPELLENT TREATMENTS ON BRIDGE DECKS
PHASE 2

FINAL REPORT ~ FHWA-OK-15-05
ODOT SP&R ITEM NUMBER 2229

Submitted to:
John R. Bowman, P.E.
Director of Capital Programs
Oklahoma Department of Transportation

Submitted by:
M. Tyler Ley, Ph.D., P.Eng.
Mehdi Khanzadeh Moradllo, Ph.D. Candidate
School of Civil and Environmental Engineering (CIVE)
Oklahoma State University

October 2015

TECHNICAL REPORT DOCUMENTATION PAGE

1. REPORT NO. **FHWA-OK-15-05**	2. GOVERNMENT ACCESSION NO.	3. RECIPIENTS CATALOG NO.
4. TITLE AND SUBTITLE **EXPECTED LIFE OF SILANE WATER REPELLANT TREATMENTS ON BRIDGE DECKS**		5. REPORT DATE **October 2015** 6. PERFORMING ORGANIZATION CODE
7. AUTHOR(S) **M. Tyler Ley, Mehdi Khanzadeh Moradllo**		8. PERFORMING ORGANIZATION REPORT
9. PERFORMING ORGANIZATION NAME AND ADDRESS **Oklahoma State University** **Civil and Environmental Engineering** **207 Engineering South** **Stillwater, Oklahoma 74078**		10. WORK UNIT NO. 11. CONTRACT OR GRANT NO. **ODOT SP&R Item Number 2229**
12. SPONSORING AGENCY NAME AND ADDRESS **Oklahoma Department of Transportation** **Materials and Research Division** **200 N.E. 21st Street, Room 3A7** **Oklahoma City, OK 73105**		13. TYPE OF REPORT AND PERIOD COVERED **Final Report** **October 2013 – September 2015** 14. SPONSORING AGENCY CODE
15. SUPPLEMENTARY NOTES		

16. ABSTRACT

This report outlines the investigation of the service life of sliane sealers on Oklahoma bridge decks as well as laboratory investigation of a silane sealer and a two part sealer that uses both silane and epoxy.

The performance of silanes on bridge decks was completed on 60 bridges that were in service between 5 to 20 years. Samples were taken from the travel lane and the shoulder. The work found that after 12 years that 100% of the silane applications were effective. By 15 years then only 68% were still effective and between 17 to 20 years then only 16% were still effective. The investigations suggest that abrasion was not a major deterioration mechanism; instead, deterioration from the high alkaline pore solution is suggested to be of importance.

This work goes on to investigate a two part system of silane and epoxy sealer, a silane, and then a control sample and their resistance to chloride penetration. Both sealers show improved performance over the sample with just concrete. Additionally, a new experimental technique is presented that is capable of non-destructively imaging the penetration of external fluids into paste and mortar. This test is rapid, accurate, and can be used for in-situ testing. This test method again shows that the silane investigated was effective at reducing the ingress of ions.

17. KEY WORDS **Silane, concrete, durability**	18. DISTRIBUTION STATEMENT **No restrictions. This publication is available from the Materials & Research Division, Oklahoma DOT.**		
19. SECURITY CLASSIF. (OF THIS REPORT) **Unclassified**	20. SECURITY CLASSIF. (OF THIS PAGE) **Unclassified**	21. NO. OF PAGES **59**	22. PRICE **N/A**

SI* (MODERN METRIC) CONVERSION FACTORS

APPROXIMATE CONVERSIONS TO SI UNITS				
SYMBOL	**WHEN YOU KNOW**	**MULTIPLY BY**	**TO FIND**	**SYMBOL**
LENGTH				
in	inches	25.4	millimeters	mm
ft	feet	0.305	meters	m
yd	yards	0.914	meters	m
mi	miles	1.61	kilometers	km
AREA				
in^2	square inches	645.2	square millimeters	mm^2
ft^2	square feet	0.093	square meters	m^2
yd^2	square yard	0.836	square meters	m^2
ac	acres	0.405	hectares	ha
mi^2	square miles	2.59	square kilometers	km^2
VOLUME				
fl oz	fluid ounces	29.57	milliliters	mL
gal	gallons	3.785	liters	L
ft^3	cubic feet	0.028	cubic meters	m^3
yd^3	cubic yards	0.765	cubic meters	m^3
NOTE: volumes greater than 1000 L shall be shown in m^3				
MASS				
oz	ounces	28.35	grams	g
lb	pounds	0.454	kilograms	kg
T	short tons (2000 lb)	0.907	megagrams (or "metric ton")	Mg (or "t")
TEMPERATURE (exact degrees)				
^oF	Fahrenheit	5 (F-32)/9 or (F-32)/1.8	Celsius	^oC
ILLUMINATION				
fc	foot-candles	10.76	lux	lx
fl	foot-Lamberts	3.426	candela/m^2	cd/m^2
FORCE and PRESSURE or STRESS				
lbf	poundforce	4.45	newtons	N
lbf/in^2	poundforce per square inch	6.89	kilopascals	kPa

APPROXIMATE CONVERSIONS FROM SI UNITS				
SYMBOL	**WHEN YOU KNOW**	**MULTIPLY BY**	**TO FIND**	**SYMBOL**
LENGTH				
mm	millimeters	0.039	inches	in
m	meters	3.28	feet	ft
m	meters	1.09	yards	yd
km	kilometers	0.621	miles	mi
AREA				
mm^2	square millimeters	0.0016	square inches	in^2
m^2	square meters	10.764	square feet	ft^2
m^2	square meters	1.195	square yards	yd^2
ha	hectares	2.47	acres	ac
km^2	square kilometers	0.386	square miles	mi^2
VOLUME				
mL	milliliters	0.034	fluid ounces	fl oz
L	liters	0.264	gallons	gal
m^3	cubic meters	35.314	cubic feet	ft^3
m^3	cubic meters	1.307	cubic yards	yd^3
MASS				
g	grams	0.035	ounces	oz
kg	kilograms	2.202	pounds	lb
Mg (or "t")	megagrams (or "metric ton")	1.103	short tons (2000 lb)	T
TEMPERATURE (exact degrees)				
ºC	Celsius	1.8C+32	Fahrenheit	ºF
ILLUMINATION				
lx	lux	0.0929	foot-candles	fc
cd/m^2	candela/m^2	0.2919	foot-Lamberts	fl
FORCE and PRESSURE or STRESS				
N	newtons	0.225	poundforce	lbf
kPa	kilopascals	0.145	poundforce per square inch	lbf/in^2

*SI is the symbol for the International System of Units. Appropriate rounding should be made to comply with Section 4 of ASTM E380.

Acknowledgments

The research team would like to thank Jeff Davis for his assistance with the μXRF analysis. We would also like to thank the Oklahoma Transportation Center and EDAX for helping to fund an equipment grant in order to purchase the μXRF Orbis equipment.

A number of personnel at ODOT were essential to this project. These include:

- Walt Peters
- Bryan Hurst
- Gary Hook
- Kenny Seward

This group helped to facilitate obtaining cores for this work and provided as technical oversight for this project.

Table of Contents

LIST OF FIGURES

LIST OF TABLES

CHAPTER 1 - INTRODUCTION

Concrete structures face a multitude of problems that threaten the serviceability of the structure, one of the largest being chloride ingress. Chlorides permeate through the concrete matrix causing corrosion of the steel reinforcement. According to a study conducted by the Federal Highway Administration (FHWA), the total direct cost of corrosion from 26 analyzed sectors was determined to be $279 billion per year in the United States. Of this total, it was estimated that $8.3 billion in damages occurred specifically to highway bridges [Koch, 2001].

One cost effective method to prevent chloride ingress is the use of protective coatings. These coatings reduce chloride ingress by either clogging the pores of the matrix thus reducing the material that permeates into the concrete, or by lining the concrete pores with a water repellent coating. An example of the latter is organosilane or silane. Silane is used by the state of Oklahoma and many others to prolong the service life of bridge decks. Although silanes have been proven to be effective at reducing the ingress of brine solutions, little work has been done to show the effective lifespan of these sealers and their long-term performance. This area will be discussed in this work. In addition, this study investigates traditional silane coatings and also novel two part coatings by using a novel micro X-ray fluorescence (μXRF) technique. Finally, a new non-destructive method using X-ray radiography is used to determine early age penetration properties of different cement systems and a silane sealer.

CHAPTER 2 - INVESTIGATION OF THE PRESENCE AND EFFECTIVE LIFESPAN OF SILANE IN CONCRETE

2.1 OVERVIEW

Silane is a commonly used surface treatment to reduce water entry into concrete. Although silanes have been proven to be effective at reducing the ingress of brine solutions, little work has been done to show the effective lifespan of these sealers and their long-term performance. The effectiveness of silanes has been suggested to decrease from ultraviolet light, physical abrasion, weathering, and alkaline attack of the hydrophobic molecules. The objective of this study was to evaluate the performance of silane sealers for 60 bridges that were in-service between 6 and 20 years in Oklahoma.

2.2 EXPERIMENTS

2.2.1 Sample Acquisition

Cores that were approximately 3/4” mm in diameter by 1” in height were taken from the driving lane and shoulder of 60 bridge decks (**Fig. 1**). Six cores were taken from each bridge for a total of 360 cores. Three cores were taken from the shoulder and three from the travel lane. These cores were taken at parallel locations so that the amount surface wear could be compared. Cores were taken from areas that were clear of debris, cracks, oil, and salt scaling damage. These cores were collected with a cordless drill. This technique allowed two researchers to sample each bridge in about 1 h. This minimized the requirement for traffic control and allowed more samples to be collected. Since the cores were small, this minimized damage and patching to the

bridges. These bridges had an age range of 6 to 20 years. Details about the sampled bridges are provided in appendix. The investigated bridges had an average annual daily traffic (AADT) between 3,600-18,000 [ODOT, 2011]. Typical weather conditions in Oklahoma are shown in **Fig. 2**.

Figure 1- Example of cores were taken from bridge decks

Although the concrete mixture designs and silanes varied, all of them were constructed to known specifications [ODOT, 2009]. The concrete mixture had a water to binder ratio of 0.42, a minimum cement content of 565 lb/yd^3 and typically contained portland cement and 20% replacement of class C fly ash as a binder. All approved silane sealers are alcohol based and used between 40% and 50% active ingredient. The specified depth of silane was 1/8" or greater and was verified by the Oklahoma Department of Transportation after construction by using a dye and visual inspection with an optical microscope from extracted cores.

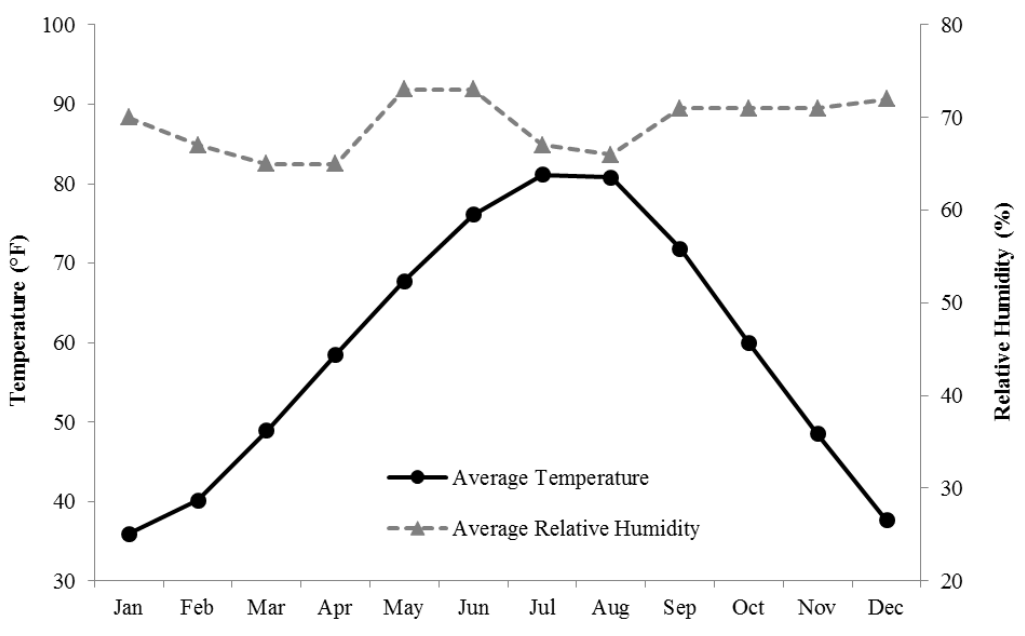

Figure 2- Variations in mean ambient temperature and relative humidity of Stillwater, Oklahoma [Oklahoma Climatological Survey, 2015]

2.2.2 Sample Preparation and Testing

A cross section of each core was exposed by polishing with 120 grit sandpaper for 5 minutes. Next, the polished surface was cleaned with ethanol to remove any dirt and residue. A new piece of sand paper was used for each sample. The samples were inspected with two techniques to determine the presence of the silane.

First, the core is ponded in blue dye (Powder Rit Dye) for 30 minutes. The dye stains the concrete that is not treated with the silane. An example can be seen in **Fig. 3b.** Past publications used X-ray fluorescent microscopy to image silane sealed concrete before and after treatment with the dye to verify the accuracy [Ley et al. 2012; Sudbrink et al. 2015]. Next, the depth of the silane was measured at six different points by using a caliper and an optical microscope and an average was reported for each core.

Then the core was polished to remove the dye from the exposed surface and then ponded in mineral based cutting oil (Rockhound oil) for 60 seconds. The oil will wet the surface of the concrete that does not contain the silane sealer. The depth is then measured as described previously with the optical microscope and calipers. Typical results are shown in **Fig. 3c**. Both methods had good agreement with one another and allowed a verification of the measurement.

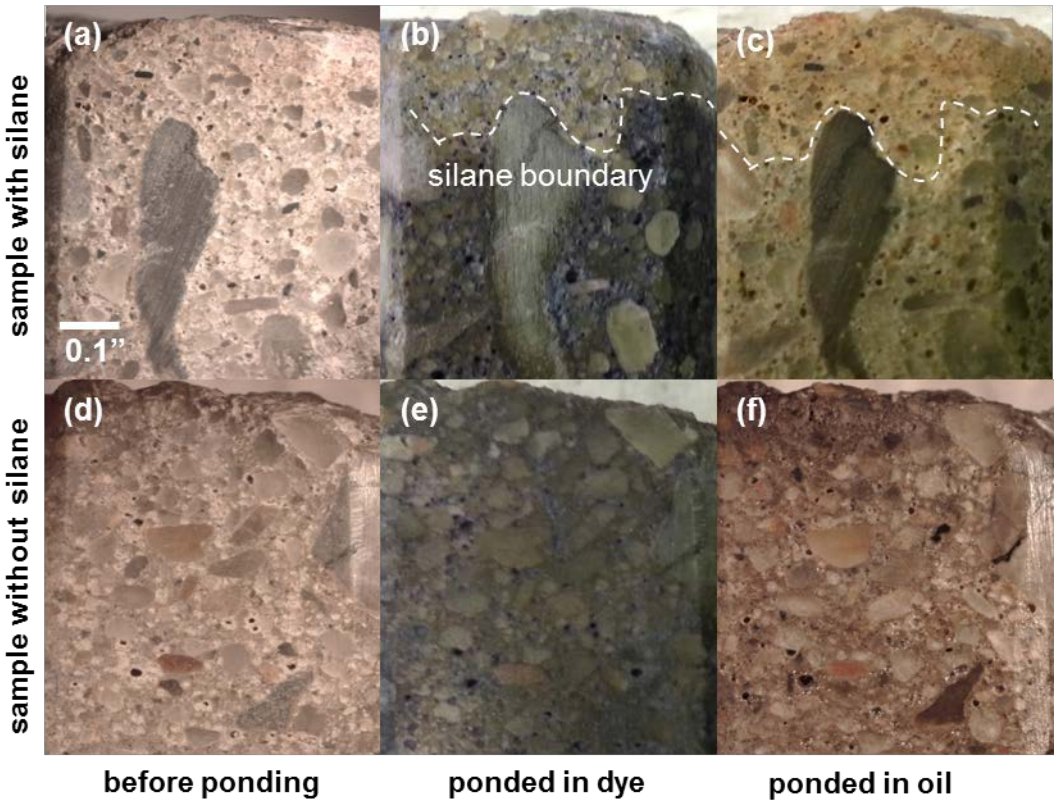

Figure 3- Example of cores before and after being ponded in the blue dye and oil: (a) core containing silane before ponding (7 year old sample) (b) core containing silane after ponding in dye (c) core containing silane after ponding in oil (d) core without silane before ponding (17 year old sample) (e) core without silane after ponding in dye (f) core without silane after ponding in oil

2.2.3 Statistical Analysis Methods

The results were statistically analyzed with an analysis of variance (ANOVA) together with a Duncan's multiple range pairwise comparison. ANOVA is an appropriate procedure for testing the equality of several means. Duncan's multiple range pairwise comparison is useful for pairwise comparison of group means. This is useful to establish the population means of two groups are statistically different from one another [Duncan, 1955; Hunter, 1978]. In the ANOVA, the dependent variable was the mean of the silane depth, and the independent variable was the age of bridge decks. The statistical analysis was undertaken to compare the average silane depths from different bridges with various ages and to evaluate the significance of difference between the averages. In addition, two-way ANOVA was used to determine the significance of difference between results of travel lane and shoulder.

2.3 RESULTS AND DISCUSSION

2.3.1 Silane Penetration Depth

Figures 4 and **5** show the average and standard deviation of the silane depth from the three cores in the travel lane and shoulder for each bridge. A horizontal line at 1/8" is shown in the graphs, as this is the minimum value required by specification and verified at construction. Based on results, all of the bridges that are less than 12 years old showed a silane depth higher than 1/8". After 15 years of service, 67% of the bridges (8/12) had a silane depth greater than 1/8". For bridges that had 17 to 20 years of service, 16% (3/19) of the bridges had a silane depth greater than 1/8".

Based on Duncan's multiple range pairwise comparison, no significant difference was found between the means of silane depth of bridges with age of 6 to 12 years. The difference between means of silane depth of bridges with 17 to 20 years of age was also not significant. Therefore, the investigated bridges were grouped into three age intervals to further discuss their performance: 6 to 12 years old, 15 years old and 17 to 20 years old.

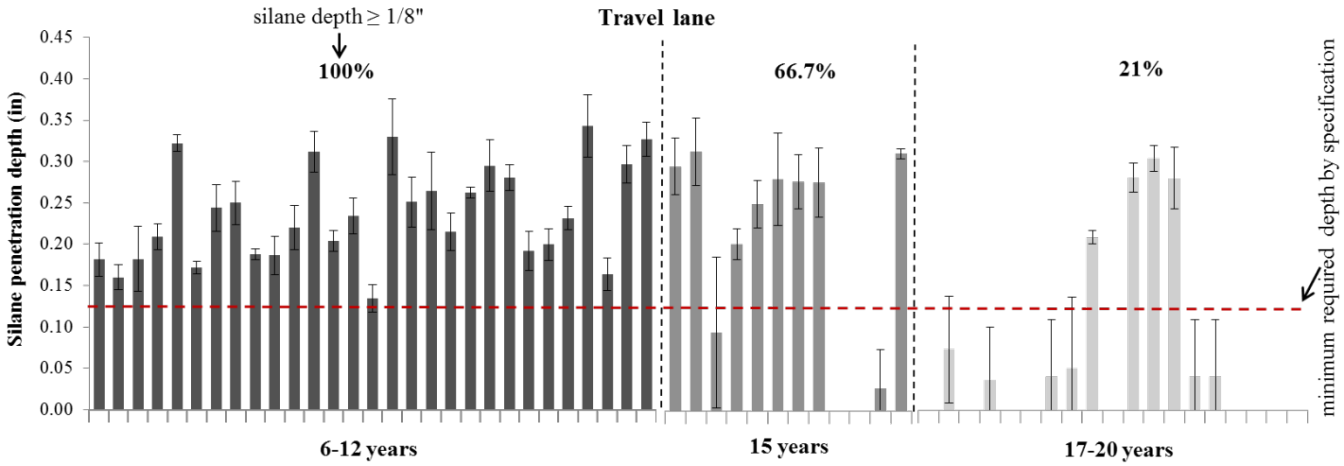

Figure 4- Average silane visual detection depth of samples from bridge decks in travel lane

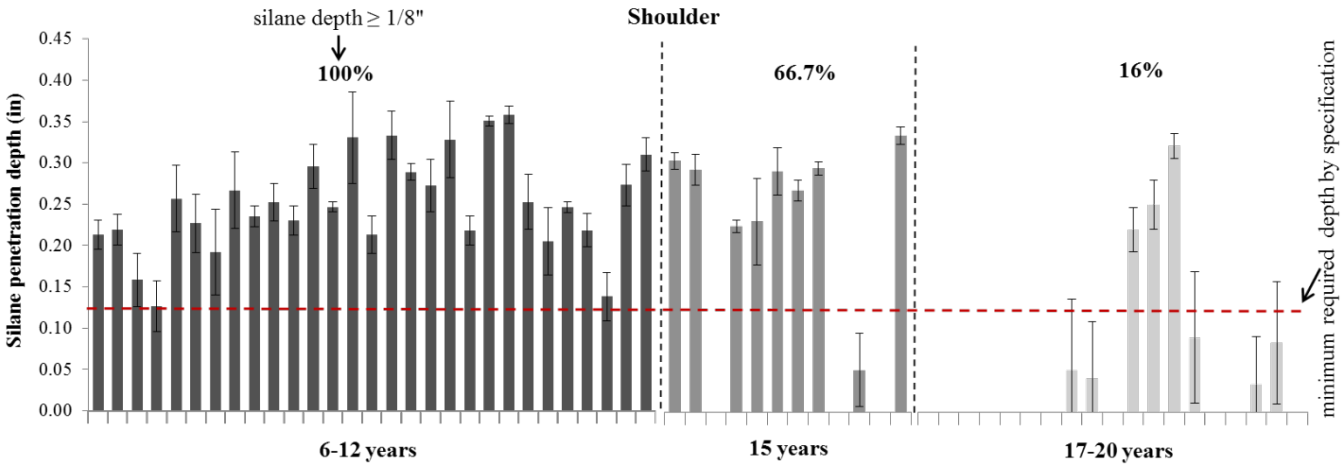

Figure 5- Average silane visual detection depth of samples from bridge decks in shoulder

Table 1 shows the average and standard deviation of the silane coating and the percentage of bridges that had coatings greater than or less than 1/8". Comparing the silane thickness to 1/8" is useful because all of the coatings should have been greater than this after construction. If the thickness is less than 1/8" then it suggests that the material may be deteriorating. This is discussed in more detail in the mechanism section.

Table 1 shows that the average depth of silane is decreasing with time for the cores from the main lane and the shoulder. After 15 years of service the average silane layer thickness reduced by 25% compared to the bridges that were less than 12 years of age. For bridges with 17 to 20 years of service, the average layer thickness reduced by 75% compared to the bridges that were less than 12 years of age.

Table 1- Summary of the number and the percentage of concrete bridge decks that still have an effective silane layer after a given service life

Years of service		6-12 years	15 years	17-20 years
Total No. of bridges		29	12	19
Travel lane	silane depth ≥ 1/8"	29 (100%)	8 (66.7%)	4 (21%)
	silane depth < 1/8"	0 (0%)	4 (33.3%)	15 (79%)
Shoulder	silane depth ≥ 1/8"	29 (100%)	8 (66.7%)	3 (16%)
	silane depth < 1/8"	0 (0%)	4 (33.3%)	16 (84%)
Travel lane	average silane depth ±std (in)	0.24±0.06	0.19±0.13	0.07±0.11
Shoulder	average silane depth ±std (in)	0.25±0.06	0.19±0.13	0.06±0.10
average difference in silane depth in shoulder and travel lane ±std (in)		0.05±0.03	0.03±0.02	0.04±0.04

Based on the ANOVA analysis, there is a probability of less than 0.01% that the silane depth of bridge decks from 6-12 years of service and 17-20 years are the same. This means there is a significant difference between the mean silane depth of the two

groups. In addition, the probability that the 15 year old and 17 to 20 year old bridges have an equal average silane depth is less than 1%.

One hypothesized reduction in silane effectiveness is removal by abrasion. The travel lanes on a bridge should receive significantly more traffic than the shoulders. By comparing the difference in between cores from these two locations then this will allow the impact of abrasion on silane thickness to be quantified. As described in the experimental methods, all comparisons between the traffic lane and shoulder are made at parallel locations and so this should be an appropriate comparison.

Figure 6 shows the difference between these two regions for each bridge and Table 1 shows the average and standard deviation of the difference between the two locations. The means and standard deviations for these measurements were similar. Based on the two-way ANOVA analysis, there is a probability of less than 10% that the mean silane depth of travel lane and shoulder is not the same. This suggests that the differences between these regions are small and that removal of the silane by abrasion was minimal over the first 20 years of service for the investigated bridges.

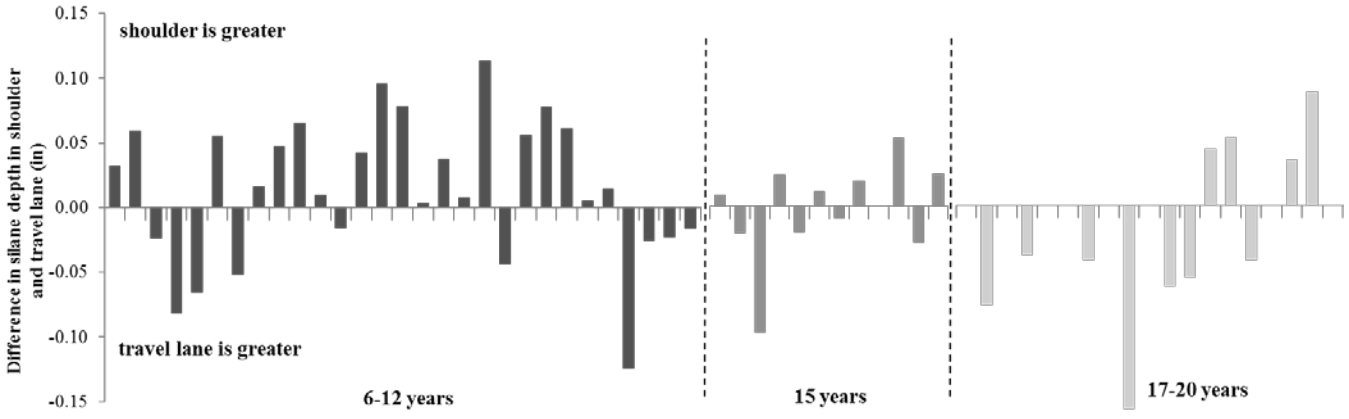

Figure 6- Difference between silane penetration depth of travel lane and shoulder

2.3.2 Mechanisms of Silane Deterioration

The result of this work shows that the average silane layer starts to decrease after 12 years of service. Several mechanisms for silane deterioration have been proposed including: ultraviolet light, physical abrasion, deterioration from external moisture, and deterioration by the alkaline pore solution [Polder et al. 2001; Selander, 20110; Dai et al. 2010; Murray, 2014]. If the silane was deteriorating from ultraviolet light or from external moisture then we would expect there to be an area at the surface of the samples where the silane would be no longer hydrophobic. An example of this is shown in **Fig. 7** from bridges that are 8 and 17 years old. However, this surface deterioration was observed in less than 5% of the samples investigated. This suggests that deterioration from ultraviolet light and external moisture is not a significant deterioration mechanism for the materials, locations, and environmental exposure investigated. Moreover since there was very little difference in the silane depth between the driving lane and the shoulder, this suggests that abrasion is also not a major contributor to the silane deterioration.

Based on **Fig. 8**, the silane deterioration seems to move from the bulk of the concrete towards the surface. This could be caused by a breakdown of silicon bonding by the alkalinity of pore solution [Murray, 2014; Tosun et al. 2008]. Tosun et al. have observed the loss of Si-O and Si-O-Si bonds of silane hydrophobic layer in high alkaline environments by using Fourier transform infrared spectroscopy (FT-IR) analysis on concrete samples. The deterioration likely initiates in the bulk of the concrete because there is a greater amount of pore solution in the non-hydrophobic region.

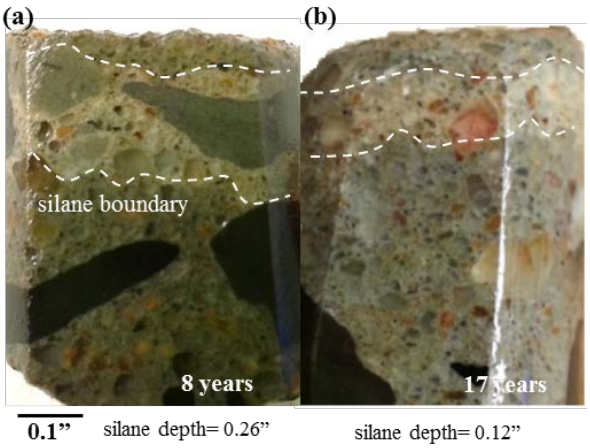

Figure 7- Example of cores with surface silane deterioration: (a) 8 year old sample with average silane depth of 0.26” (b) 17 year old sample with average silane depth of 0.12”

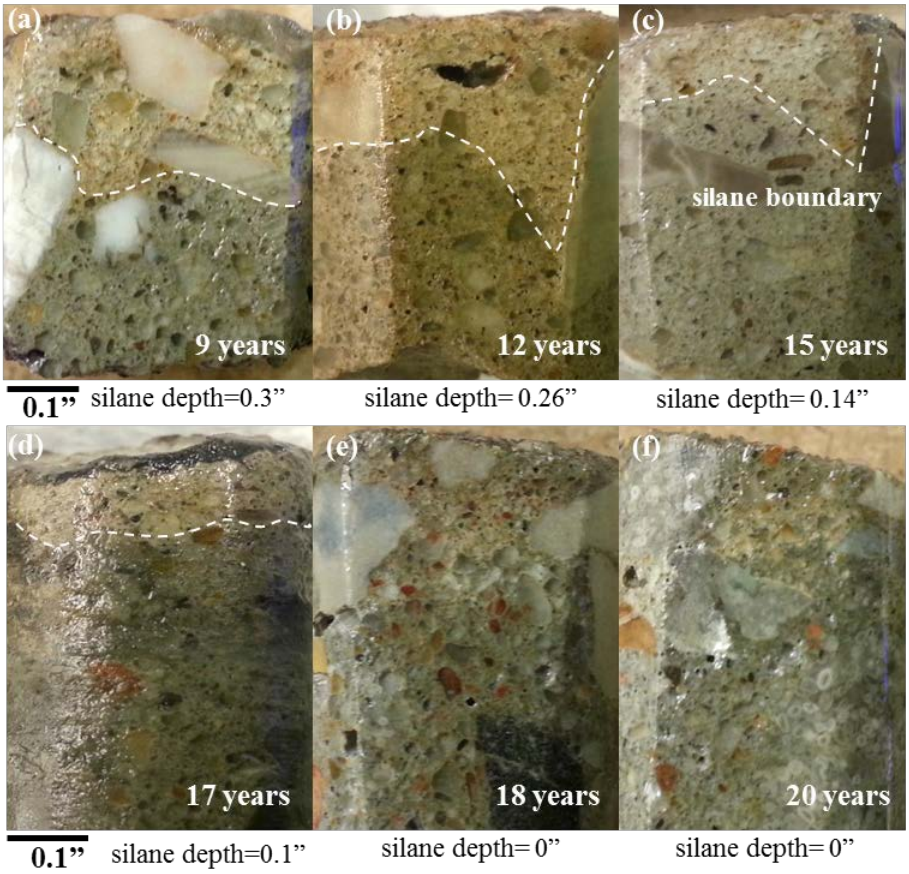

Figure 8- Example of cores with different ages being ponded in the oil: (a) 9 year old sample with average silane depth of 0.3” (b) 12 year old sample with average silane depth of 0.26” (c) 15 year old sample with average silane depth of 0.14” (d) 17 year old sample with average silane depth of 0.1” (e) 18 year old sample without silane (f) 20 year old sample without silane

2.3.3 Practical Recommendations

This work shows that silane sealers provide a hydrophobic surface on the concrete for about 12 years and then the thickness starts decreasing for the bridge decks investigated. Since the deterioration of the silane appears to be related to the alkaline pore solution, then one would expect similar performance in other locations and environments but at different rates depending on the average temperature and possibly humidity. However, mixtures that use higher dosages of supplementary cementitious materials (SCMs), such as fly ash, slag, and silica fume, may see an even larger lifespan, as these materials are known to produce lower amounts of calcium hydroxide from dilution of portland cement and consume calcium hydroxide during their reaction. By decreasing the calcium hydroxide then this should decrease the alkalinity of the pore solution and possibly delay the attack on the silane sealer, and possibly prolong the life of the material. This is an area of future study.

Other literature has suggested that silane should be reapplied at intervals of 10–20 years to stay effective [Freitag and Bruce, 2010; Sandeford et al. 2009]. Unfortunately, there is very little data about the effectiveness of reapplying silane or the expected lifespan of this new coating. This reapplication would be a function of the cleanliness of the concrete surface, exposure conditions, and the concrete quality. More research is needed to investigate these recommendations in field conditions.

2.4 CONCLUSION

This work used 360 cores from 60 concrete bridge decks with ages between 6 and 20 years that were treated with silane in order to determine the effective service life

of silane treatments. Two different optical staining techniques were used on these cores to determine the average penetration of the silane with visual contrast.

The following observations were made:

• After 12 years of service, 100% of the bridge decks in the driving lane and the shoulders were found to have a silane layer greater than the minimum specified value of 1/8”

• After 15 years of service, only 68% and after 17 to 20 years only 16% of the bridges showed evidence of a silane layer greater than 1/8” in thickness

• The average depth of silane starts to decrease after about 12 years of service in both the main lane and the shoulder. For bridges with 15 and 17 to 20 years of service, the average silane layer thickness reduced by 25% and 75% respectively compared to the bridges that were less than 12 years of age

• The silane thickness was similar for the samples from the travel lane and shoulder for all bridges. This suggests that abrasion was not a significant deterioration mechanism of the silane coating for these structures

• Less than 5% of the field samples showed deterioration of the silane sealer at the surface of the concrete. This suggests that damage from ultra violet light and external moisture was not significant, and the deterioration by the alkaline pore solution appears to be a more important silane deterioration mechanism for these materials and exposure level

Silane sealers are a useful tool to help extend the service life of structural concrete. This work has shown that these materials have a limited lifespan and the

results suggest that the deterioration is likely caused from the alkaline pore solution. More work is needed to understand how these findings translate to different environments and concretes.

CHAPTER 3 - APPLICATION OF MICRO X-RAY FLUORESCENCE (μXRF) TO STUDY THE SILANE RESISTANCE TO PENETRATION OF CHLORIDE IONS

3.1 OVERVIEW

The most prevalent and costly durability problem with structural concrete is the corrosion of internal reinforcing steel from chloride ions. One cost effective method to extend the service life of concrete is to use hydrophobic sealers that decrease the penetration of fluids. Organosilanes or silanes are commonly used to water-proof the pores. A wide range of silane sealers are currently available for protection of concrete. However, the availability of various silanes makes the right selection difficult since they can provide different levels of protection. This chapter uses micro X-ray fluorescence (μXRF) to compare the Cl penetration resistance of the new two-part silane-epoxy system with a widely used type of silane in Oklahoma. μXRF is a non-destructive chemical imaging technique which measures Cl profile with less human effort and provides important insights not possible with the typical profile grinding analysis.

3.2 EXPERIMENTS

3.2.1 Materials

A concrete mixture with a water-to-cementitious ratio (w/cm) of 0.45 was investigated in this chapter. An ASTM C618 Class C fly ash is used as 20% of the mass of the binder. The cement is an ASTM C150; Type I. The chemical composition of cementitious materials is in **Table 2** and was obtained by bulk XRF. The coarse aggregate is a dolomitic limestone and the fine aggregate is a locally available natural

sand. Two different sealers, an Alkyltrialkoxysilane (SIL-ACT, ATS-42) and two-part silane-epoxy system (DECK-SIL 1700) from Advanced Chemical Technologies of Oklahoma City, are used to seal and waterproof concrete surfaces. The properties of applied silanes are given in **Table 3**.

Table 2- Chemical composition with bulk XRF

Binder	Cement	Fly ash
SiO_2 (%)	20.40	38.71
Al_2O_3 (%)	5.03	18.82
Fe_2O_3 (%)	2.95	5.88
CaO (%)	62.89	23.12
MgO (%)	2.08	5.55
Na_2O (%)	0.35	1.78
K_2O (%)	0.35	0.58
TiO_2 (%)	0.28	1.35
MnO_2 (%)	0.10	0.02
P_2O_5 (%)	0.16	1.46
SrO (%)	0.16	0.39
BaO (%)	0.12	0.72
SO_3 (%)	3.05	1.27
L.O.I (%)	2.09	0.35
Moisture (%)	0.16	0.11

Table 3- Properties of applied silanes

Type	Chemical type	Solid content (by weight)	Density (lb/gal)	Application rate (ft^2/gal)
ATS-42	Alkyl trialkoxy silane	> 40%	6.76	125-250
DECK-SIL PS1700	Alkyl trialkoxy silane	100%	7.68	100

3.2.2 Mixture Proportion and Sample Preparation

The concrete mixture was prepared according to ASTM C192. All of the aggregate, both coarse and fine, were brought into the temperature controlled mixing

facility at least a day before and their batch weights were corrected based on their moisture content. The aggregates were charged into the mixer along with approximately two-thirds of the mixing water. The combination was mixed for 3 min. Next, the walls of the mixer were scraped to remove material that stuck to the walls. Then the cement and fly ash was loaded into the mixer, followed by the remaining mixing water. The mixer was turned on for 3 min. Once this mixing period was complete, the mixture was left to ‘‘rest’’ for 2 min while buildup of material along the walls was removed. Next the mixer was run for 3 min. After mixing, the slump, unit weight, and the air content were measured according to ASTM C143, ASTM C138, and ASTM C231, respectively. The concrete mixture proportion is given in **Table 4**.

The concrete was placed in 4 x 4 x 3 inch plastic molds. The samples were sealed cured for seven days at 73°F. Three samples were used for each sealer type and three samples as a control without any sealer. Next, all the samples were dried in an environmental chamber with a temperature of 73°F and 40% relative humidity for 70 days. Then the sample surface was cleaned to remove any residue before application of sealers.

Table 4- Concrete mixture proportion

Material	Cement (lb/yd^3)	Fly Ash (lb/yd^3)	Coarse Agg. (lb/yd^3)	Fine Agg. (lb/yd^3)	Water (lb/yd^3)	w/cm
Content	488.8	122.2	1835	1195	275	0.45

3.2.3 Silane Application

After drying period, all edges of the samples were sealed with wax. Then three samples were ponded with an ATS-42 type silane and three others with DECK-SIL

PS1700 type silane for 1 h. By trial and error it was found that after 1 h of ponding the 0.45 w/c concrete had a depth of ATS-42 type silane penetration of 1/8”.

Next, the surface of samples with the DECK-SIL PS1700 was dried for 30 minutes at 73°F and 40% relative humidity before applying the epoxy sealer at the surface. The manufacturer instructions were followed for mixing and applying the EP 1700 with a brush. A fine aggregate was then broadcast on the sample surface to follow the field application procedure. Weights of samples are measured before and after ponding with silane and epoxy to determine the amount of penetrated silane and the application rate of epoxy polymer. Then all samples were dried in an environmental chamber at 73°F and 40% relative humidity for 21 days after silane application.

3.2.4 Ponding in Sodium Chloride Solution

After drying, the area between the concrete and the container was sealed with wax and the specimen was then stored in lime solution for three days. This was done to fill the surface pores with lime water. The weight before and after saturation was measured to determine a mass change after ponding. Next, the specimen was ponded with 10.3 lb/ft^3 aqueous sodium chloride solution according to ASTM C1556 for 45 days at 73°F. After the ponding period, the Cl solution was removed and the samples were stored for 24 hours in laboratory conditions. Then, samples were cut and the exposed cross section was polished on a sanding belt for 5 minutes with 120 grit sandpaper to create a flat surface. Ethanol was then used to remove dirt and residue from the polished surface. This flat surface allowed for easier interpretation of the μXRF and optical microscopy results.

3.2.5 µXRF Procedure

The µXRF analysis was conducted using the Orbis by EDAX. The instrument uses an 80 mm² Silicon Drift Detector Energy Dispersive Spectrometer (SDD-EDS) and a capillary optic that produces a 50 µm diameter beam. Images are created by moving the sample under the stationary X-ray beam. The X-ray beam causes characteristic fluorescence X-rays to be emitted at each spot, the intensity of these characteristic X-rays are measured by the SDD-EDS and stored in a database for later processing and analysis. **Table 5** summarizes the settings used by the µXRF in this work. More details can be found in other publications [Ley et al. 2012; Sudbrink et. al. 2015].

Table 5- Summary of µXRF settings used

counts per second	minimum of 20,000
current	1000 mA
dead time	maximum of 20%
dwell time	400 ms/pixel
Filter	25 µm Al
vacuum	1.35 Torr
voltage	40 keV

Next, a set of reference standards were used to develop a calibration curve to change the count data to Cl concentration. This was done by making concrete samples with known amounts of NaCl. The samples were then cured for seven days, polished, and then cleaned as described previously.

3.2.6 Determining Silane Depth of Penetration

After cutting the samples, a cross section was exposed by polishing with 120 grit sandpaper for 5 minutes. Then the sample is ponded in water for 60 s to determine hydrophobic region. Next, the depth of the silane was measured at six different points

by using a caliper and an optical microscope and an average was reported for each sample. This is the same procedure as was used previously.

3.3 µXRF DATA ANALYSIS

3.3.1 µXRF Raw Data

Typical raw data from µXRF is shown in **Fig. 9**. An optical image is shown along with individual elemental maps. The different light levels in the optical image are caused by different normalization while stitching the images together. The elemental maps show areas with higher concentrations by using brighter pixels. These maps can be misleading. If there is an area of high concentration then it will appear much brighter than other areas. This can give the illusion that the concentration is almost zero in other locations. This can be resolved by the clustering analysis presented in the next section.

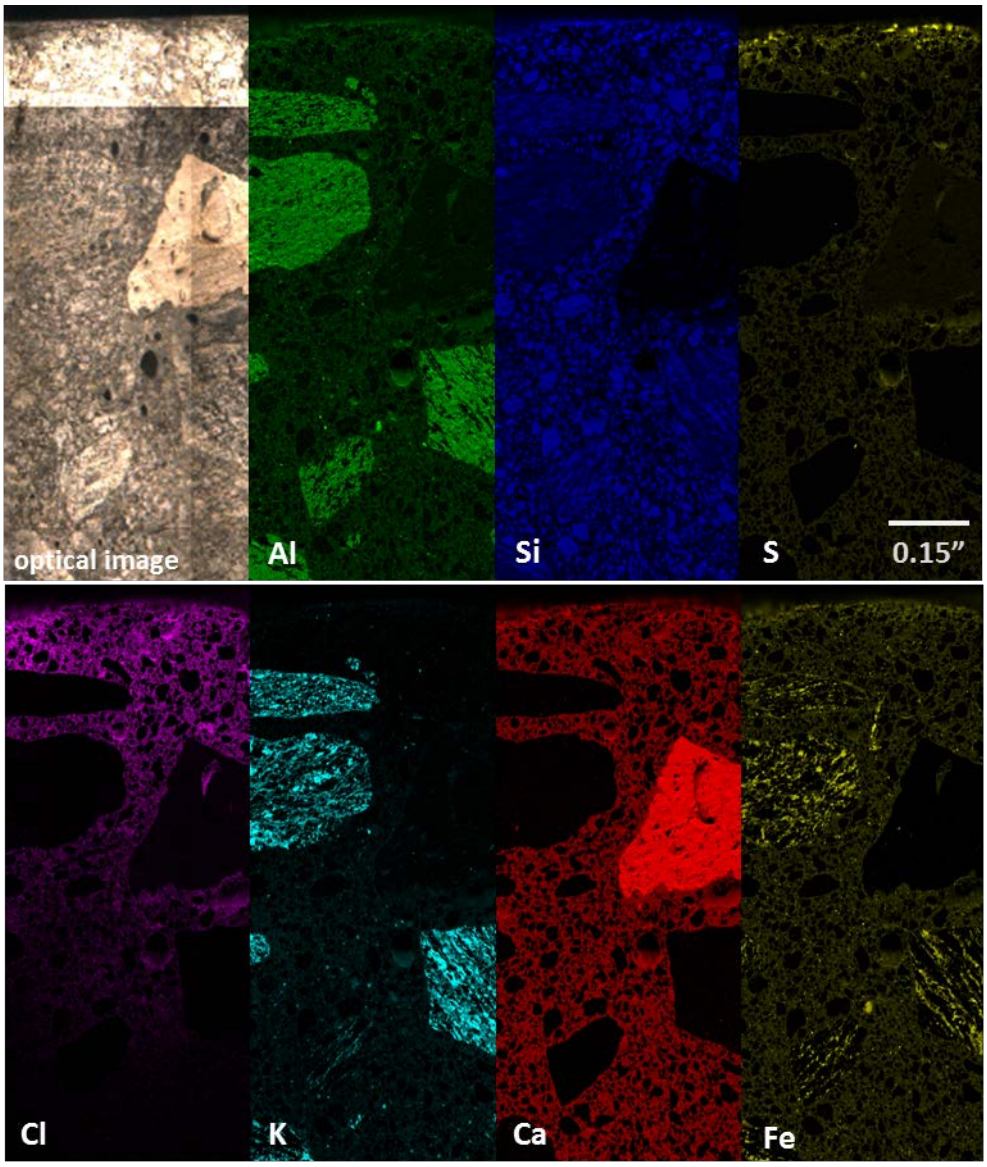

Figure 9- Example of elemental images provided by µXRF

3.3.2 Cluster Analysis

After each sample is scanned with µXRF, the compositional maps were analyzed with Lispix [Bright, 2011]. This program groups areas of similar composition, which are referred to as clusters. This analysis is helpful as one can combine individual compositional maps into a single map that simultaneously provides unique compositions and location. This separation of unique regions is useful in data display and analysis.

A cluster was determined by using the optical and elemental images to define unique regions. For example aggregates were determined based on high counts of elements such as Si (for silicate aggregates) and Ca (for limestone aggregates) as shown in **Fig. 10**. Next, the cement paste was defined and separated by different elemental concentration levels (i.e., different levels of Cl), as shown in **Fig. 11**. Once the paste and the aggregate phases were marked, they were encoded as binary masks, assigned color mappings, and plotted on the same figure as shown in **Fig. 12**. These final images provide a complete separation of the different types of aggregates, and Cl levels in the paste and is useful for qualitative observations. Additional details can be found in a previous publication [Sudbrink et al, 2015].

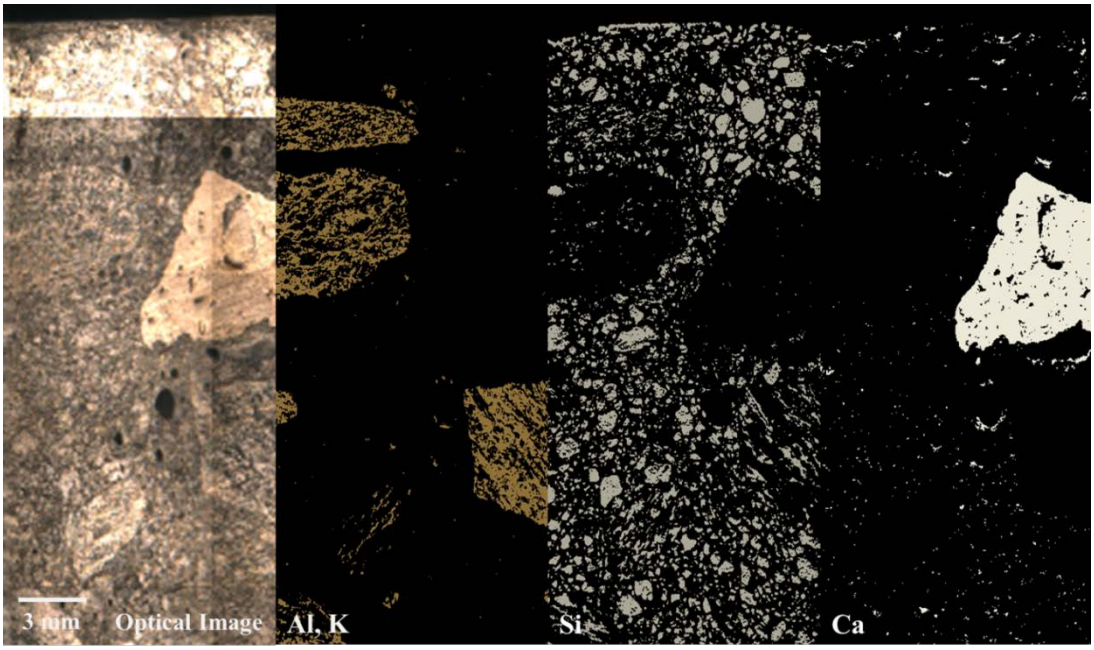

Figure 10- Example of various types of aggregates are categorized into individual clusters. Optical image (Left), cluster of aggregates rich in Al and K (middle left), cluster of siliceous aggregate (middle right), cluster of Ca rich aggregate (right). The different light levels in the optical image are caused by different normalization while stitching the images together

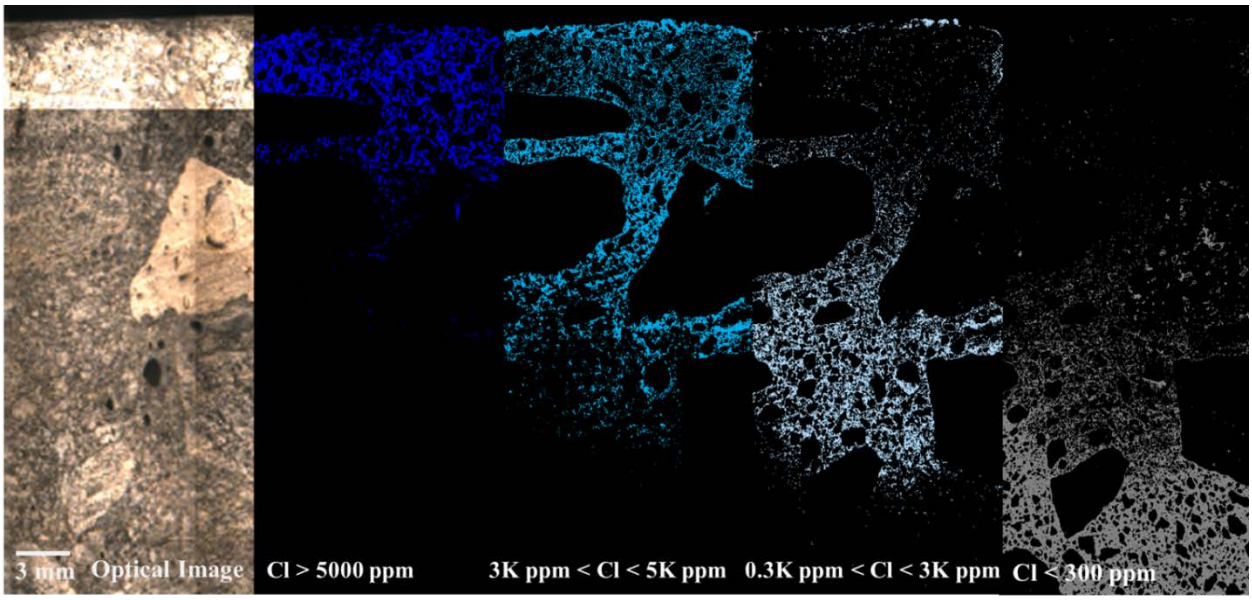

Figure 11- Example of clustering cement paste based on varying levels of Cl concentrations. Optical image (left), Cl concentration higher than 5000 ppm (middle left), Cl concentration between 3000 and 5000 ppm (middle), Cl concentration between 300 and 3000 ppm (middle right), and Cl concentration less than 300 ppm (right). The different light levels in the optical image are caused by different normalization while stitching the images together

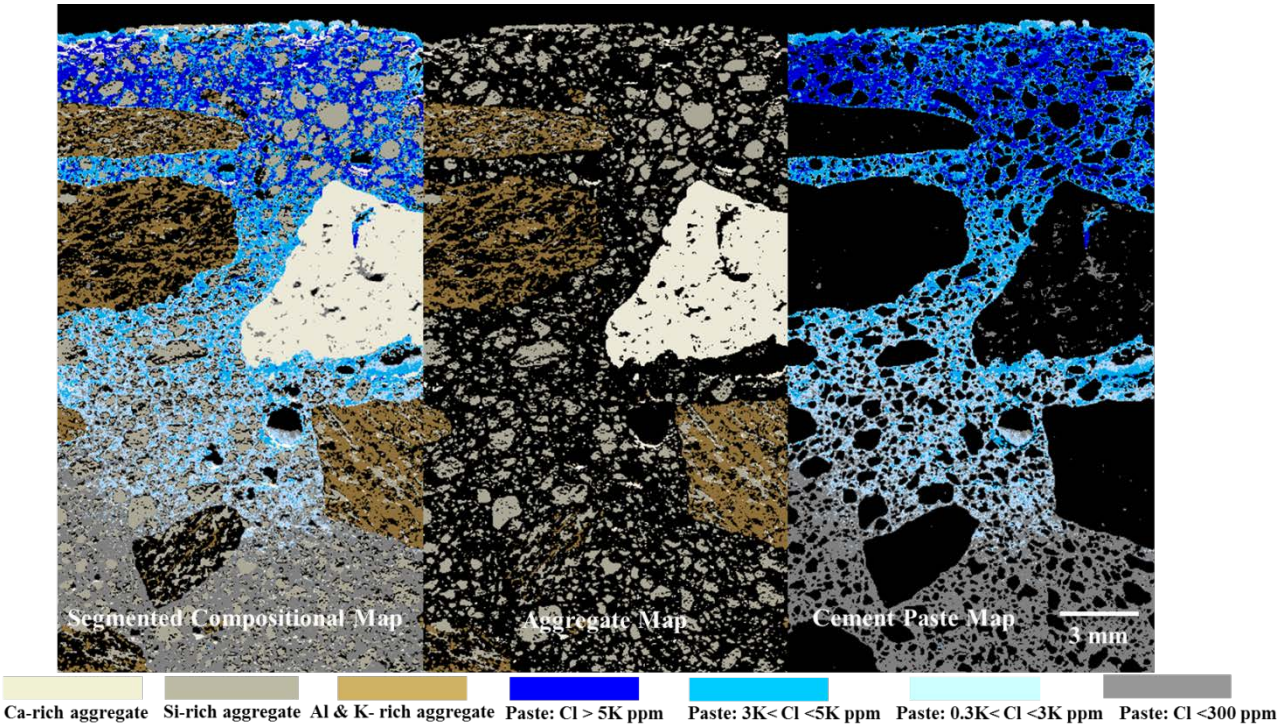

Figure 12- An example of a compositional map showing the aggregate and paste: (left), aggregate (middle), and cement paste (right)

3.3.3 Quantitative Analysis of μXRF Data

Finally, a self-authored computer code was used to analyze the spatial and compositional data. An overview of the program is shown in **Fig. 13**. First, the segmented image of the sample is used to remove the aggregates and isolate the paste. This is helpful so that the Cl concentration contributed by the aggregate and paste can be compared. A border detection algorithm is used to find the top surface of the sample. The sample is then separated into 0.02” layers of equal thickness from the surface of the sample through the entire depth as shown in **Fig. 13d**. The average Cl amount in each layer can then be plotted for different depths.

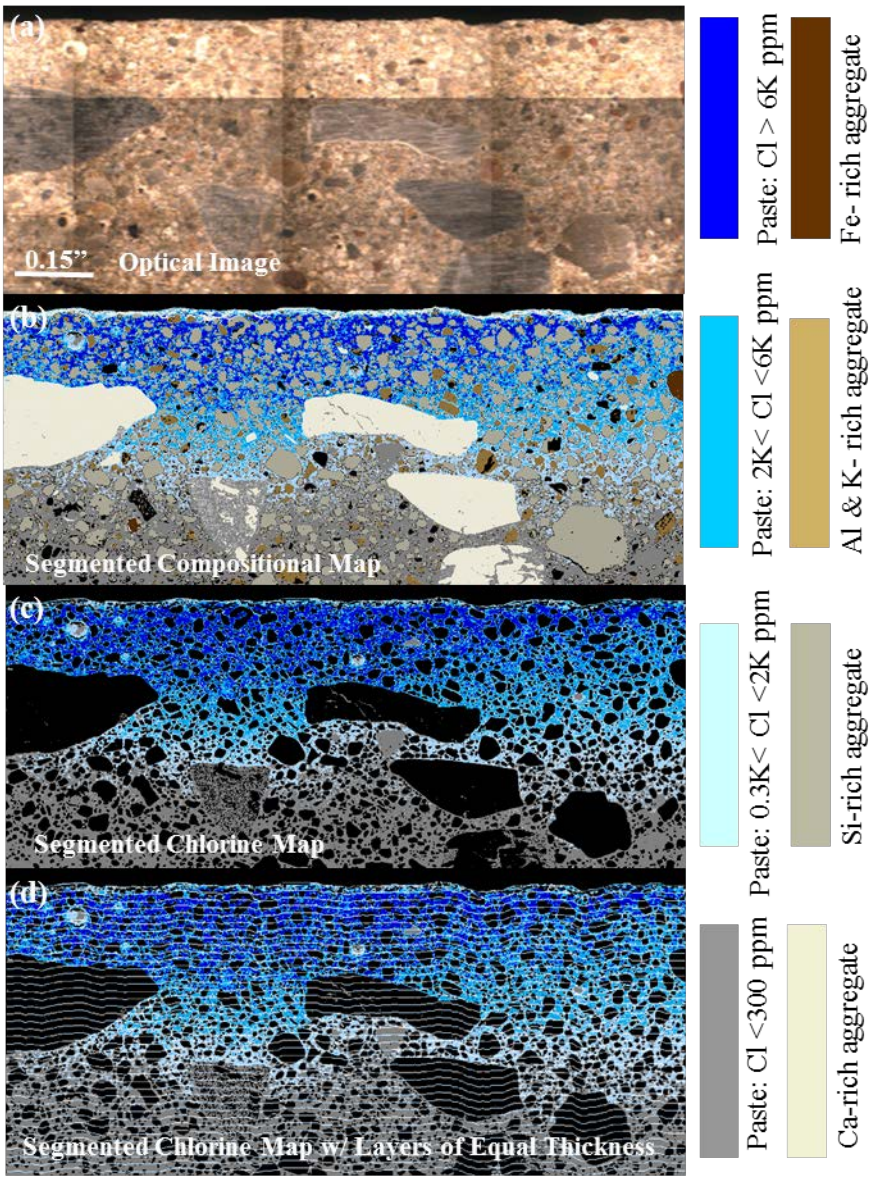

Figure 13- An example of using the self-authored program to remove the aggregates and divide the sample into layers of equal thickness from the surface: (a) optical image (b) segmented compositional map (c) segmented Cl profile map (d) segmented Cl profile map with layers of equal thickness

3.4 RESULTS

3.4.1 Silane Application Rate and Penetration Depth

The penetration depth and amount of material based on mass change are given in **Table 6**. In addition, **Figure 14** illustrates the silane penetration depth for samples

with different sealer types. Based on weight change after applying the epoxy polymer on treated samples with DECK-SIL PS1700, the application rate of epoxy polymer is 0.78 lb. per sq. ft. The PS1700 had 20% more penetration than ATS-42. This greater penetration could be due to differences in the formulations of PS1700 and ATS-42 or the reduction in evaporation caused by the epoxy coating used with the PS 1700. More work on this topic is needed to draw further conclusions.

Table 6- Silane application rate and penetration depth

Sealer type	ATS-42	PS 1700
Ave. silane uptake (% Wt sample)	0.21±0.02	0.31±0.02
Ave. silane penetration depth (in)	0.14±0.01	0.17±0.01

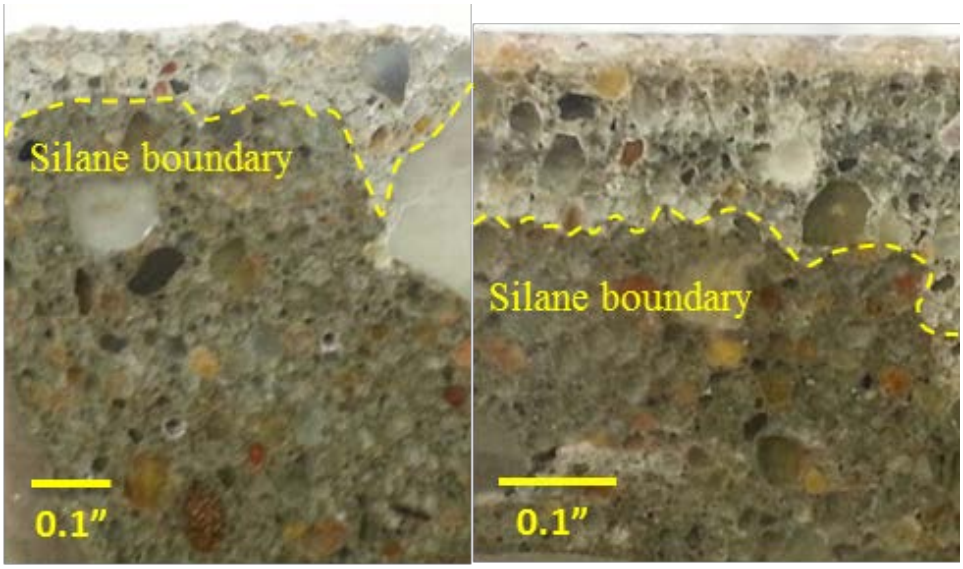

Figure 14- Silane penetration depth: (left) concrete sample with ATS-42 type silane (average penetration depth=0.14”) (right) concrete sample with DECK-SIL PS1700 type silane (average penetration depth=0.17”)

3.4.2 Mass Change after Ponding in Lime Water

The average mass change of specimens are compared in **Fig. 15**. Results show that applying either sealer systems reduced water uptake by about seven times when compared to the control samples. The samples with DECK-SIL 1700 showed a little higher water uptake than samples with ATS-42 type silane. This could be due to the water absorption by the sand placed on the surface of the PS 1700.

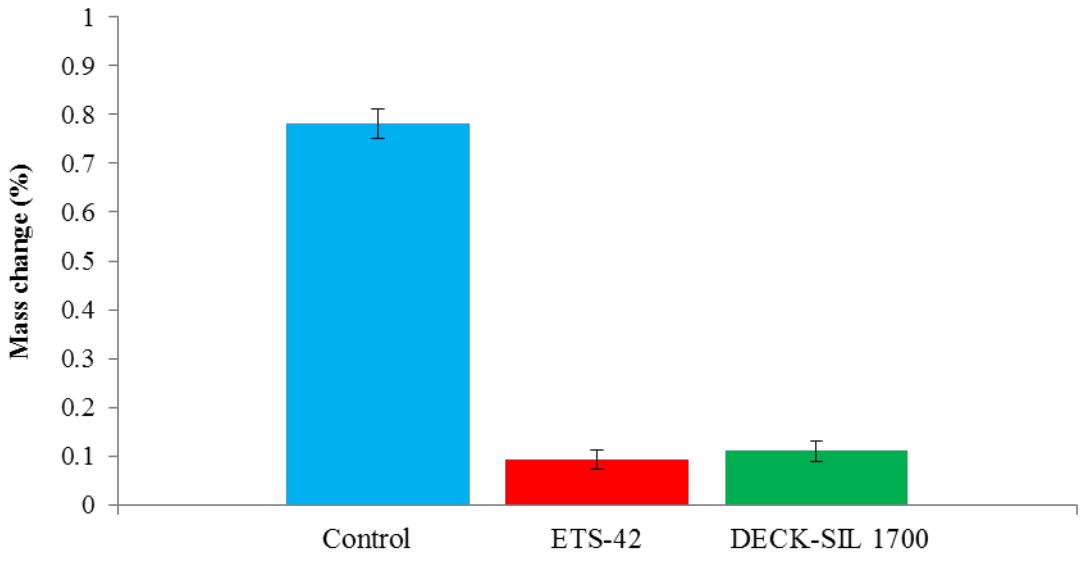

Figure 15- Mass change of different samples after ponding in lime water

3.4.3 Compositional Maps from μXRF

A segmented constituent and paste map is shown in **Fig. 16**. Both of the sealers showed significant reduction in the Cl penetration into the concrete samples.

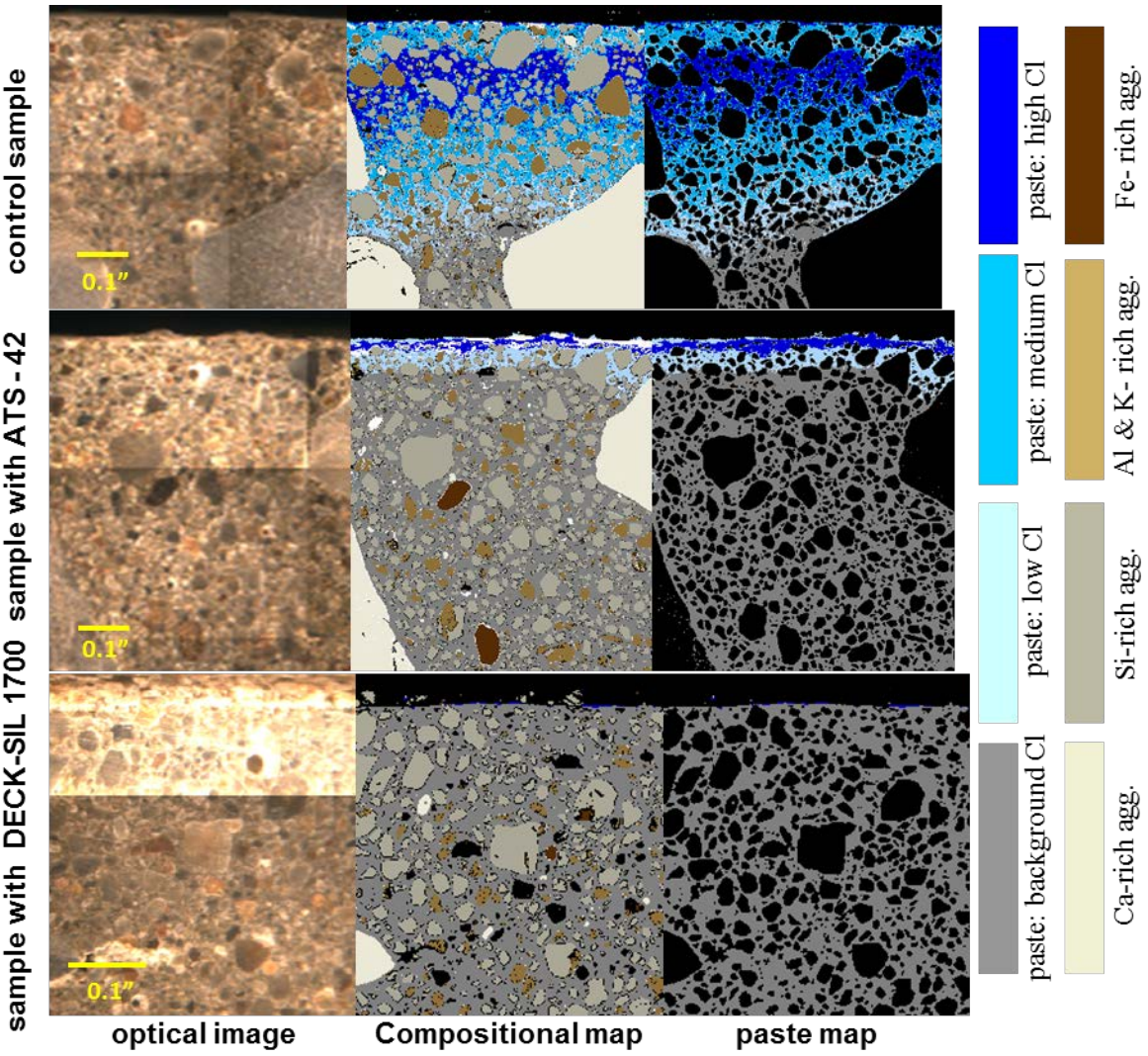

Figure 16- Compositional and paste maps of different samples

3.4.4 Cl Concentration Profiles from µXRF

Based on µXRF quantitative analysis, Cl concentration profiles of the samples are shown in **Fig. 17**. The Cl profiles confirm the results of the segmented maps and provide a quantitative measurement. In the control sample, Cl penetrated up to 1/2", while Cl penetration depth is limited to 0.1" in the ATS-42 samples and almost immeasurable amounts of penetration for DECK-SIL 1700.

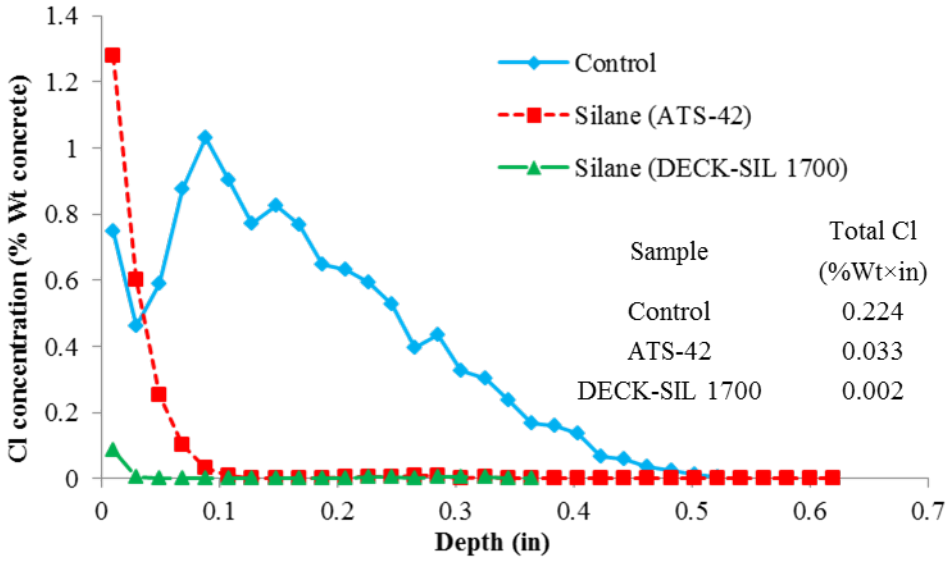

Figure 17- Cl concentration profiles of different samples and total Cl uptake

3.5 DISCUSSION

The PS1700 showed a 20% deeper penetration than ATS-42. This may provide a longer effective life if deterioration from high alkaline pore solution. The long-term performance of this two part sealer was not studied in current study. More research is needed to investigate this sealer long-term durability.

The ATS-42 reduced Cl penetration by five times when compared to the control sample and the DECK-SIL 1700 showed almost immeasurable amounts of Cl penetration. This suggests the DECK-SIL 1700 two part system seems to show superior abilities to resist Cl penetration. In addition, the ATS-42 and DECK-SIL 1700 reduced total Cl uptake about 85% and 99% when compared to the control sample, respectively. This superior performance of DECK-SIL 1700 could be influenced by the ability of the epoxy topcoat to seal the surface cracks of the sample, this is an area of future study.

3.6 CONCLUSION

In this chapter, a micro X-ray fluorescence (μXRF) is used to compare the Cl penetration resistance of two sealer systems in comparison to concrete without the sealer. The following observations were made:

• The two-part silane-epoxy sealer system (DECK-SIL 1700) 20% greater penetration when compare to a silane commonly used in Oklahoma (ATS-42) when they were applied in the same manner on the same concrete.

• After 45 days of ponding in NaCl, the ATS-42 reduced the depth of Cl penetration by five times when compared to the control sample.

• The DECK-SIL 1700 showed negligible penetration of Cl after 45 days of ponding in NaCl.

• The ATS-42 and DECK-SIL 1700 reduced total Cl uptake about 85% and 99% when compared to the control sample, respectively.

This work shows the utility of using μXRF to efficiently and rapidly evaluate Cl profiles in concrete samples and compare the effectiveness of different sealers.

CHAPTER 4 - APPLICATION OF X-RAY RADIOGRAPHY TO STUDY DIFFUSIVITY OF IONS IN CONCRETE

4.1 OVERVIEW

Concrete structures face many threats to their service life. A number of durability problems are caused by external fluids penetrating into concrete. This fluid can lead to damage from staining, corrosion, sulfate attack, bulk freezing and thawing, and scaling. So, there is a need to develop a fast and convenient laboratory method which is able to evaluate the penetration properties of concrete samples and coating systems used on concrete. This chapter presents a new technique, X-ray radiography, to image the movement of fluid into concrete. This technique will be helpful to understand the effectiveness of different coatings systems that are used for concrete such as silane.

4.2 X-RAY RADIOGRAPHY

It is common in the medical sciences to use X-ray radiographs to non-destructively image the internal structure of organisms. In these radiographs, solid materials with different chemistry and densities will appear to have different gray values depending on their chemistry and density. Radiography uses an X-ray source, an object and a detector as shown in **Fig. 18**. The photons produced by an X-ray source penetrate through a sample. The X-rays are attenuated as they pass through the sample and the emerging or transmitted X-ray intensity is measured and recorded by the detector. This data is called a radiograph. A radiograph is a composite image of the signal as it passes through the sample. This means that the 3D features of the sample are displayed as a single image. This could be a problem if the samples contain a

number of complicated features, but these samples have been designed to have a simple geometry.

To make the water more electron dense and less transparent to X-rays, a salt is mixed into the water. The salt will dissolve in the water and the ions will in turn increase the electron density of the water. As the salt water penetrates into the cement paste it is possible to see the corresponding changes in gray value of the material in the radiograph. By observing the rate of penetration into the sample then an effective permeability can be estimated.

This means we can observe where and at what rates fluids move within the cement systems. This can help us nondestructively determine the permeability of cement paste and the performance of different surface coatings.

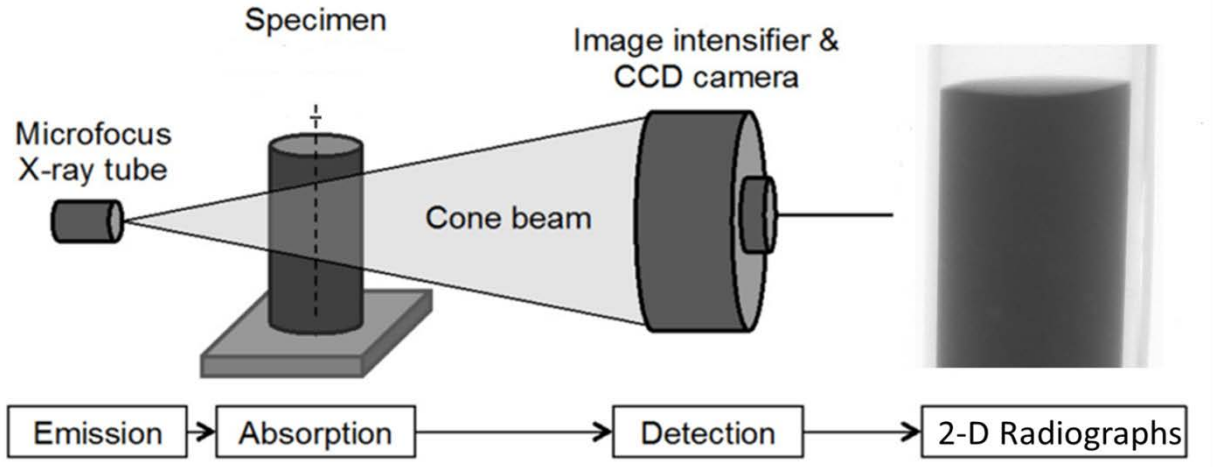

Figure 18- Overview of X-ray radiography

4.3 EXPERIMENTS

4.3.1 Mixture Proportion and Sample Preparation

Three different cement paste mixtures with water-to-cement ratio (w/c) of 0.35, 0.4, and 0.45 and one mortar mixture with w/c ratio of 0.4 were investigated in this chapter. The paste mixtures were made to compare the performance of mixtures with different w/c and the mortar mixture was conducted to measure the effectiveness of silane in reducing ion entry into the samples with X-ray radiography. The cement is an ASTM C150; Type I. the fine aggregate is a locally available natural sand. A silane (SIL-ACT, ATS-42) from Advanced Chemical Technologies of Oklahoma City is used to seal the mortar sample. The chemical composition of cement and properties of the silane are provided in chapter 3.

The paste and mortar mixtures were prepared according to ASTM C305 and the mixture proportions are given in **Table 7**. Micro vials with inside diameter of 0.375“ and a lid were used to cast the samples. Two samples from each mixture were made for the study. These samples were then cured for 28 days in a sealed condition at 73°F. The mortar samples were cured for 7 days in a sealed condition at 73°F and later dried at 73°F and 40% relative humidity for 14 days. Next, one of mortar samples was ponded with silane for 1 h and then allowed to dry for 24 hours before ponding with solution. This ponding time was chosen because by trial and error it was found that after 1 h of ponding the 0.40 w/c concrete had a depth of ATS-42 type silane penetration of 1/8”, a

required depth of penetration by Oklahoma Department of Transportation. Another mortar sample was used as control sample without a treatment.

Table 7- Paste and mortar mixtures proportions

Mixture	Water (lb)	Cement (lb)	Fine aggregate (lb)	W/C
P-1	0.82	1.82	-	0.45
P-2	0.76	1.89	-	0.40
P-3	0.69	1.96	-	0.35
M	0.37	0.91	1.83	0.40

4.3.2 Testing Procedure

To visualize the moisture penetration in materials using radiography, it is necessary to use enough salt to cause a large enough contrast difference between the fluid and the solids. In this study potassium iodide solution (KI) is used in the water placed on top of the hydrated cement paste and mortar as shown in **Fig. 19**. This salt is easy to obtain and does not require special handling requirements. After curing, paste samples were ponded with 10% (0.6 mol/L) KI solution for 28 days. The mortar samples were also ponded with a 10% KI solution for 40 days. A laboratory Skyscan 1172 mCT scanner was used to conduct experiments. A radiograph was taken from the paste and mortar samples immediately after the ponding and then again over time to determine the changes in the sample. The radiograph used a pixel size of 9 µm and voltage of 100 KeV. A filter (Al+Cu) was used to absorb lower energy X-rays and allow high energy X-rays to interact with the sample. An aluminum wire of known thickness was placed in every scan. This wire served as an alignment guide and detects variations in X-ray transmissions between images. In addition, a plastic plate was attached below the

sample to keep samples height constant between radiographs. The schematic diagram of a diffusion test setup is shown in **Fig. 19**.

After the ponding period, the solution was removed from surface of sample and the final radiograph was taken. Next, the sample was polished for further analysis with μXRF. A detailed procedure of conducting experiment with μXRF is provided in chapter 3.

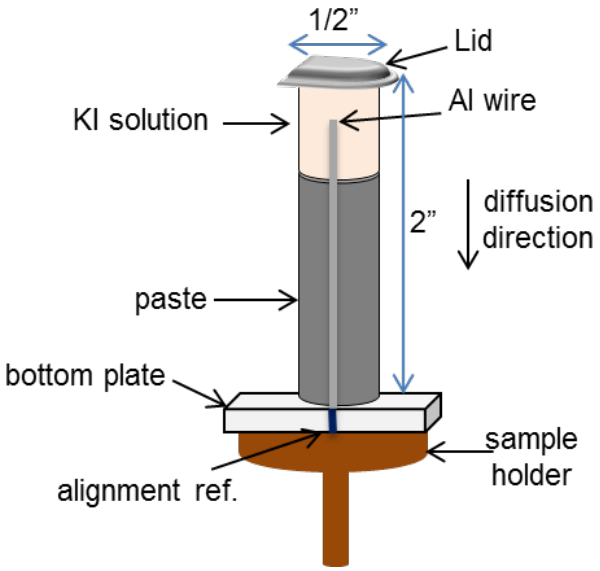

Figure 19 – Schematic diagram of the diffusion test setup

4.4 DATA ANALYSIS

As mentioned, a reference radiograph was collected immediately after ponding and time-series radiographs were collected during the ponding to determine iodide time-series concentration profiles. After collecting radiographs, the blank background subtraction was applied on time-series and reference radiographs by using the self-authored image analysis code in MATLAB to remove the background attenuation effects. Then, an average gray value profile was calculated through the sample depth

for different images by using the ImageJ v 1.48. Next, ten scan lines were used to measure the gray value with depth as shown in Fig. 20. Next, radiographs were taken at different time periods and then subtracted from the reference radiograph. This allowed the change in the gray value to be easily observed and the spatial changes due to absorption from the iodide solution to be mapped. **Equation (1)** was used to calculate a change in attenuation due to iodide mass in pore spaces ($\Delta\mu$) at different depths of sample

$$(\Delta\mu)_x = \ln(I_{ref})_x - \ln(I_t)_x \qquad (1)$$

where $(I_{ref})_x$ is the transmitted X-ray intensity (gray value) at depth x on the reference profile and $(I_t)_x$ is the transmitted X-ray intensity at the same distance on the time=t profile. This means the equation is the change in the attenuation due to iodide in the pores is equal to the natural log of the transmitted X-ray intensity minus the natural log of the reference intensity.

Next, to determine iodide concentration profiles a set of reference paste standards with different iodide concentrations were used for each paste mixture to develop a calibration curve to convert the measured $\Delta\mu$ values to concentration. The same sample size, mixtures, and scan setup were used in the experiments and to develop the calibration curves. After radiograph measurements, the control samples were polished and then analyzed with μXRF to validate the results.

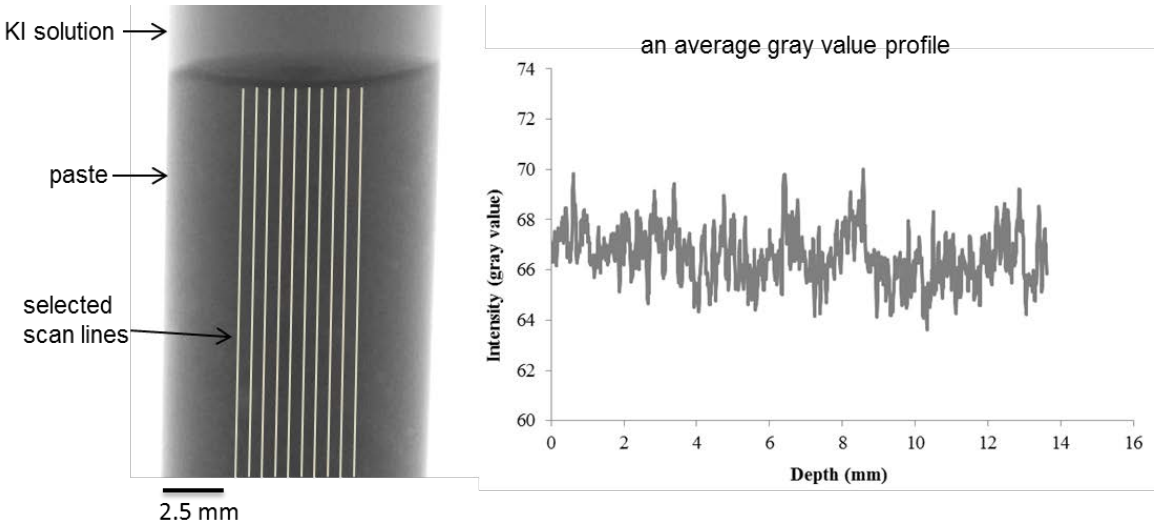

Figure 20 – An example of collected radiographs: (left) selected scan lines to average gray value through the sample depth (right) an average gray value profile

4.5 RESULTS AND DISCUSSION

4.5.1 Time-Series Radiographs

Figure 21 presents an example of radiographs taken from paste sample during ponding. Based on **Fig. 21**, the gray value of the paste changes with penetration of the solution and a time-dependent iodide diffusion front is determined from the radiographs. It is interesting that the iodide penetration depth can be estimated within minutes by using this technique.

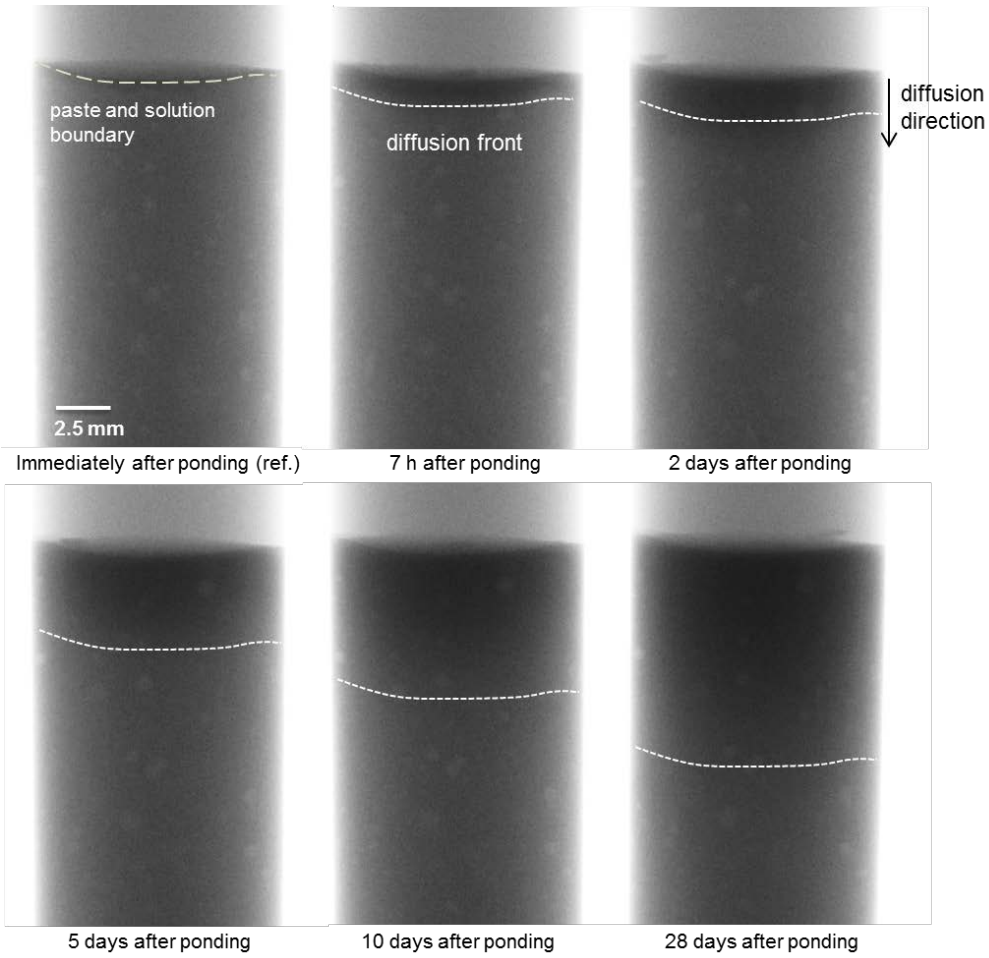

Figure 21- Example of reference and time-series radiographs (w/c=0.35)

4.5.2 Time-Series Concentration Profiles

Figure 22 displays an example of time-series concentration profiles calculated from their corresponding radiographs during ponding. In addition, measured concentration profiles of different paste mixtures are compared in **Fig. 23**. Based on **Fig. 22**, the concentration change over time at different depths and the penetration depth can be easily quantified by using this technique. According to **Fig. 23**, these radiographs provide a good comparison of the resistance of paste samples with different w/c against iodide penetration within a few hours.

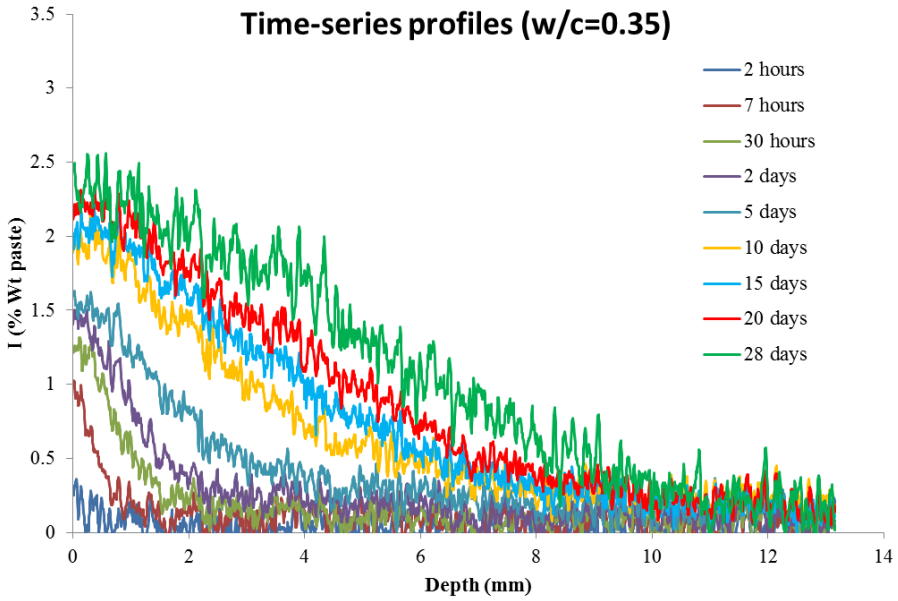

Figure 22- Example of time-series concentration profiles (w/c=0.35)

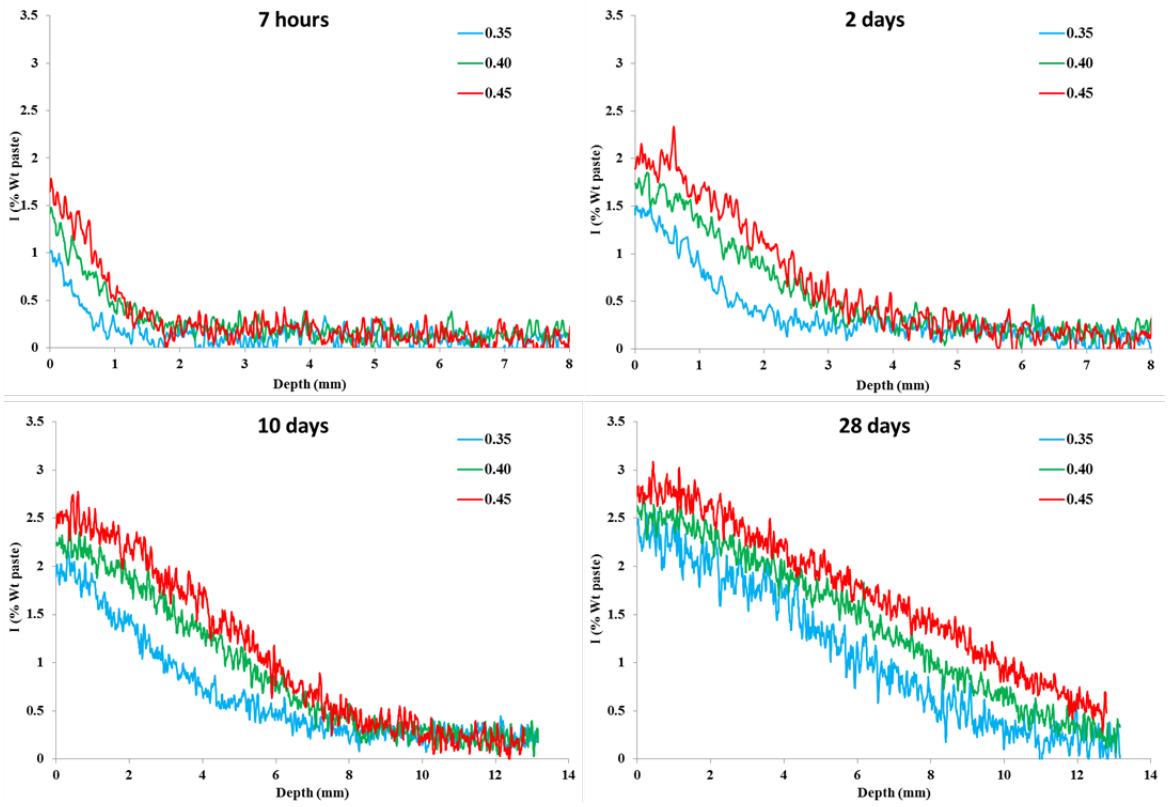

Figure 23- Comparison of concentration profiles of different paste mixtures over time

4.5.3 Comparison between radiograph and µXRF results

As mentioned, paste samples were polished and analyzed with µXRF after 28 days ponding to determine the accuracy of results from radiograph technique. **Figure 24** presents a comparison between these two methods for different w/c. Based on the results, a good correspondence was found between these techniques. Therefore, X-ray radiography is a reliable method to study a performance of different cement systems against ions intrusion with a rapid and non-destructive method. The X-ray radiography method does not provide a direct chemistry measurement, but by using standards one can take measurements in about one minute to measure the current penetration of the salt solution. Another advantage of the method is that the experiment can be conducted in-situ.

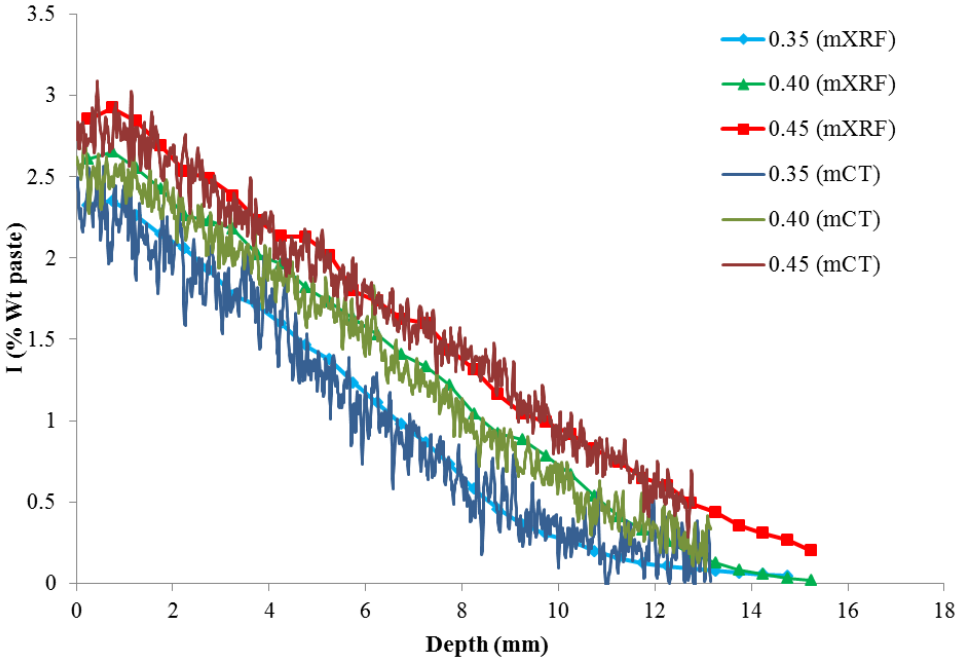

Figure 24- Comparison between radiograph and µXRF results

4.5.4 Silane Sealer Performance

As discussed, X-ray radiography can be very useful to understand the effectiveness of different coatings systems that are used for concrete. **Figure 25** displays radiographs of mortar samples with and without silane treatment after 40 days ponding with KI solution. Based on images, the mortar sample with silane showed a good resistance against the salt solution penetration compared to the control mortar sample without silane. In the control sample, the salt solution has penetrated through the entire depth of the sample. However, in the silane treated sample the penetration is about 1 mm from surface. In addition, concentration profiles from radiograph images were determined and presented for mortar samples in **Fig. 26**. The concentration profiles are in agreement with visual observations from the radiographs. Based on the radiograph images, the silane has effectively reduced ion penetration. It is interesting to note that the mortar without silane after 5 hours of exposure showed a higher concentration then the silane sample that was exposed for 40 days. This shows the usefulness of the method and the usefulness of the silane to promote long life structures.

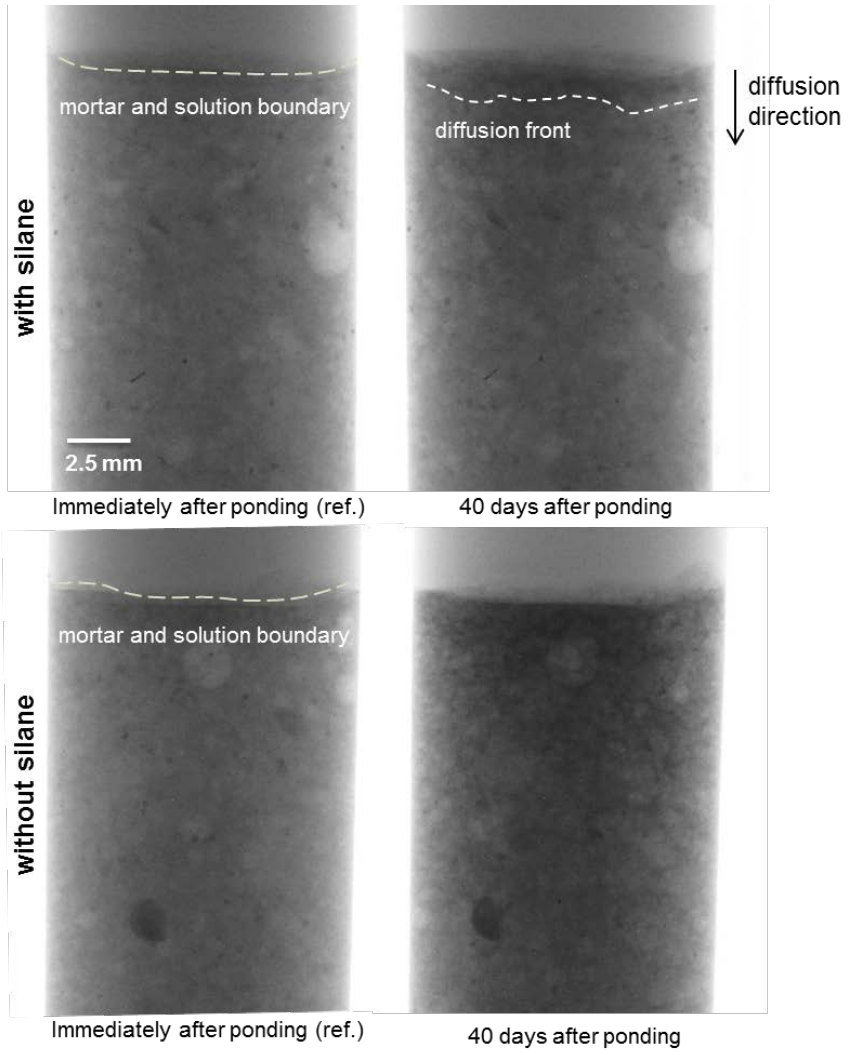

Figure 25- Radiographs of mortar samples with and without silane

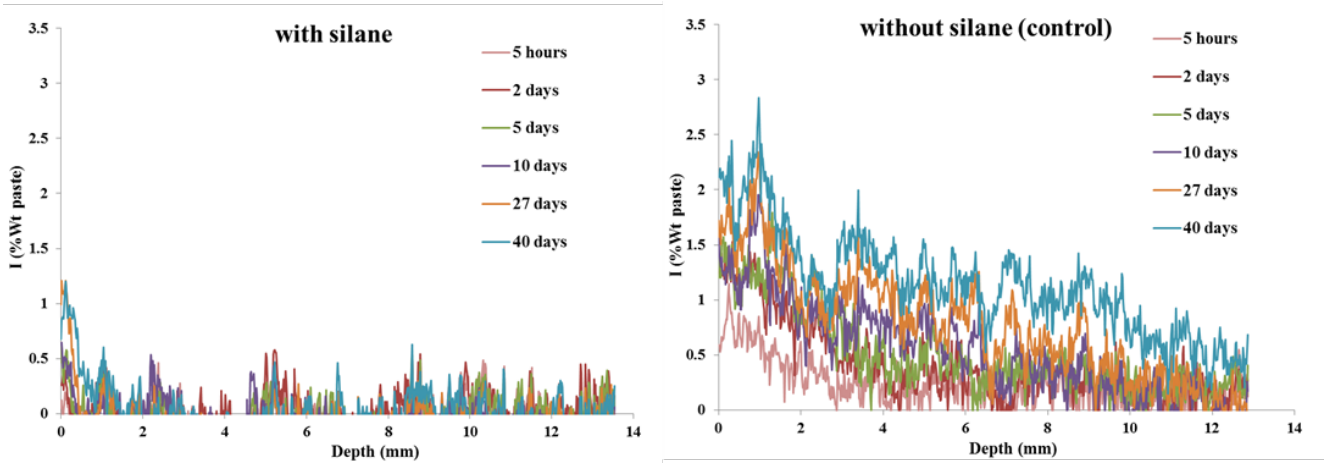

Figure 26- Time-series iodide profiles of mortar samples with and without silane

4.6 CONCLUSION

From the results, X-ray radiography is a powerful, non-destructive, imaging technique is capable of providing valuable information about the penetration of ions into paste and mortar. These techniques can be completed at different ages and with a number of different systems. These results provide useful insights not easily obtained with other methods.

The radiography method also shows outstanding agreement with the μXRF measurements from Chapter 3. The validation of the method by a totally different procedure should build confidence in the validity of the method.

The use of radiography offers advantages over conventional measurement of diffusion coefficients. By measuring time-dependent diffusion profiles in the sample, radiography allows the estimation of the penetration properties of sample at early ages. This can save time in developing the quality of the material. The ability to image the distribution of the fluid is also useful as it can be used to detect preferential pathways for diffusion or assess the influence of heterogeneity.

CHAPTER 5 - CONCLUSION

Silane sealers are a useful tool to help extend the service life of structural concrete. This work has shown that these materials perform for at least 12 years and then by 15 years only 68% of bridges showed satisfactory performance. This work also shows that the deterioration of silane is likely caused from the alkaline pore solution. More work is needed to understand how these findings translate to different environments and concretes.

The new two-part silane-epoxy system (DECK-SIL 1700) increased silane penetration depth about 20% compared to the other sealer used (ATS-42). Both of the silane systems have significantly reduced Cl penetration into concrete samples. However, the two part silane-epoxy system (DECK-SIL 1700) showed negligible Cl penetration after 45 days in the solution. More work is needed to understand the long-term performance of new two part system but the preliminary data looks promising.

A new technique that uses X-ray radiography is used to image the early age penetration of salt solutions into different cement systems. This technique is useful, rapid, and non-destructive and has proven to be useful to compare mixtures with different w/cm and to evaluate sealers such as silane.

REFERENCES

Agbogun, H.M.D., Tom A. Al, and Esam H. "Three dimensional imaging of porosity and tracer concentration distributions in a dolostone sample during diffusion experiments using X-ray micro-CT." *Journal of contaminant hydrology* 145 (2013): 44-53.

Atkinson, A., and Nickerson, A.K. "The diffusion of ions through water-saturated cement." *Journal of Materials Science* 19.9 (1984): 3068-3078.

Basham, Kim, and John Meredith. "Measuring water penetration." *Magazine of Masonry Construction* 8.11 (1995): 539-543.

Cavé, Lisa, Tom Al, Yan Xiang, and Peter Vilks. "A technique for estimating one-dimensional diffusion coefficients in low-permeability sedimentary rock using X-ray radiography: Comparison with through-diffusion measurements." *Journal of contaminant hydrology* 103.1 (2009): 1-12.

Christodoulou C., Goodier C.I., Austin S. A., Webb J., Glass G.K. “Long-term performance of surface impregnation of reinforced concrete structures with silane.” *Construction and Building Materials*, 48 (2013):708–716.

Dai J.G., Akira Y., Wittmann F.H., Yokota H., Zhang P. “Water repellent surface impregnation for extension of service life of reinforced concrete structures in marine environments: the role of cracks.” *Cement and Concrete Composites* 32(2010): 101-109.

Darma, Ivan Sandi, Takafumi Sugiyama, and Michael Angelo B. Promentilla. "Application of X-ray CT to study diffusivity in cracked concrete through the observation of tracer transport." *Journal of advanced concrete technology* 11.10 (2013): 266-281.

Duncan D.B. “Multiple range and multiple F tests.” *Biometrics* 11(1955): 1-42.

Freitag S.A., Bruce S.M. “The influence of surface treatments on the service lives of concrete bridges.” *NZ Transport Agency research report* 403, 2010, 91pp. ISBN 978-0-478-36420-0.

Hunter W.G., Hunter J.S. “Statistics for experimenters: an introduction to design, data analysis, and model building.” New York: *Wiley*; 1978.

Koch, Gerhardus H., Michiel P.H. Brongers, Neil G. Thompson, Y. Paul Virmani, and Joe H. Payer. "Corrosion Costs and Preventive Strategies in the United States"

report by CC Technologies Laboratories, Inc. to Federal Highway Administration (FHWA), Sept. 2001.

Ley M.T., Sudbrink B., Kotha H., Materer N., and Apblett A. "Expected Life of Silane Water Repellant Treatments on Bridge Decks." *Research & Development Division Oklahoma Department of Transportation*. No. FHWA/ODOT-2229 (Dec. 2012).

Murray C. “Durability of silane sealer in a highly alkaline environment.” In: MSc thesis. *University of Arkansas*; 2014.

Oklahoma Department of Transportation, Planning & Research Division, Engineering Services Branch/Data Analysis Section, Annual Average Daily Traffic Maps 2011. http://www.okladot.state.ok.us/Maps/aadt/index.htm, (last accessed on August 2015)

Oklahoma Department of Transportation. Standard Specifications Book 2009. http://www.okladot.state.ok.us/cnstrctengr.htm, (last accessed on August 2015).

Polder R.B., de Vries H. “Prevention of reinforcement corrosion by hydrophobic treatment of concrete.” *Heron* 46 (2001): 227–238.

Sandeford P., Bendell G., Mansoor A. “Corrosion management strategy for reinforced concrete wharf infrastructure located at the mouth of the Brisbane River.” *Corrosion and Materials* 34(2009): 32–37.

Selander A. “Hydrophobic impregnation of concrete structures: Effects on concrete properties.” In: Ph.D. thesis. *Royal Institute of Technology, Stockholm*, Sweden; 2010.

Sudbrink B., Khanzadeh-Moradllo M., Hu Q., Ley M.T., Davis J.M., Materer N., Apblett A. “Using micro x-ray fluorescence to image silane coatings in concrete.” *Cement and Concrete Research* (2015), Submitted for publication.

The Oklahoma Climatological Survey. Temperature and relative humidity averages: 1971-2003. <http://climate.ok.gov/index.php/climate/category/oklahoma_climate> (last accessed on August 2015).

Tosun K., Felekoglu B., Baradan B. “Effectiveness of alkyl alkoxy silane treatment in mitigating alkali-silica reaction.” *ACI Materials Journal* 105 (2008):20–7.

Bright D. “Lispix: An image processing and analysis tool for the PC.” 2011. http://www.nist.gov/lispix/doc/contents.htm, (last accessed on August 2015).

APPENDIX

Table A1- Location and details of investigated bridges

No.	Structure No.	Bridge ID	Facility Carried	Bridge Name	Years of service	County	Division	AADT
1	5220 0066 X	28472	SH 15	Creek	6	Nobel	4	4800
2	5233 2144EX	28181	I-35 NB	Red Rock Creek-North		Nobel	4	15400
3	4204 1287 X	28479	US 77	Beaver Creek		Logan	4	5600
4	1904 2105 X	28655	SH 66	Rock Creek		Creek	8	7500
5	1904 2139 X	28654	SH 66	Rock Creek O'Flow		Creek	8	7500
6	3210 0216 X	28133	US 270	Salt Creek		Hughes	3	3600
7	3628 0101 X	27813	SH 11	Turkey Creek	7	Kay	4	5900
8	1908 0709 X	28539	SH 75A	Childers Creek		Creek	8	5800
9	5706 1850 X	27838	US 60	Buck Creek		Osage	8	3800
10	5706 1927 X	27837	US 60	Turkey Creek W		Osage	8	3800
11	5706 1943 X	27836	US 60	Turkey Creek		Osage	8	3800
12	6732 0778WX	27081	SH99	Turkey Creek		Seminole	3	4300
13	6737 1804 X	28808	SH 56	I-40 UNDER		Seminole	3	4200
14	0220 0745 X	26715	SH 11	Salt Fork 1	8	Alfalfa	6	3800
15	3625 1501 X	27772	SH 11	I-35 UNDER-West		Kay	4	5900
16	5737 0721 X	27812	SH 97	Delaware Creek TRIB.		Osage	8	3800
17	5737 0739 X	27811	SH 97	Delaware Creek		Osage	8	3800
18	3212 0826 X	27748	SH 9	Little Wewoka Creek-1		Hughes	3	3600
19	3212 0844 X	27747	SH 9	Little Wewoka Creek-2		Hughes	3	3600
20	4455 0040 X	28033	SH 24	Finn Creek		McClain	3	4000
21	0220 0780 X	26716	SH 11	Salt Fork 2	9	Alfalfa	6	3800
22	0220 0799 X	26717	SH 11	Salt Fork 3		Alfalfa	6	3800
23	0220 0820 X	26718	SH 11	Salt Fork 4		Alfalfa	6	3800
24	0220 0842 X	26719	SH 11	Salt Fork 5		Alfalfa	6	3800
25	0220 0891 X	26720	SH 11	Sandy Creek		Alfalfa	6	3800
26	0220 0920 X	26721	SH 11	Powell Creek		Alfalfa	6	3800
27	0220 0933 X	26722	SH 11	Creek		Alfalfa	6	3800
28	4208 1097NX	26281	SH 33	Fitzgerald Creek-1	12	Logan	4	7100
29	4208 1097SX	26280	SH 33	Fitzgerald Creek-2		Logan	4	7100
30	3616 1975 X	25596	US 177	Shoefly Creek	15	Kay	4	4500
31	5220 1062 X	26443	SH 15	Long Branch Creek		Nobel	4	3600
32	5220 0632 X	26444	SH 15	Legend Creek		Nobel	4	3600
33	2506 1080 X	25818	US 177	Spring Brook Creek 1		Garvin	3	3800
34	2508 0551 X	25272	SH 19	Washita River		Garvin	3	4400

No.	Structure No.	Bridge ID	Facility Carried	Bridge Name	Years of service	County	Division	AADT
35	2508 1022 X	25273	SH 19	Deep Creek		Garvin	3	4400
36	2508 1474 X	25392	SH 19	Beef Creek		Garvin	3	4400
37	2512 1597 X	25233	SH 19	Spring Brook Creek 2		Garvin	3	4400
38	0905 3465NX	25888	Reno	I-40 FRTG. RD. WB		Canadian	4	18000
39	0905 3465SX	25889	Reno	I-40 FRTG. RD. EB		Canadian	4	18000
40	0912 0205WX	26237	US 81	U.S. 81-Canadian River		Canadian	4	6400
41	4902 0539WX	25503	US 69	Brush Creek		Mayes	8	13700
42	0905 3306 X	25127	Czech	Czech Hall RD.	17	Canadian	4	6200
43	4906 0422 X	25715	SH 20	Seminole Creek		Mayes	8	8200
44	4906 0489 X	25718	SH 20	Pryor Creek		Mayes	8	8200
45	4906 0509 X	25719	SH 20	Creek		Mayes	8	8200
46	0912 0063 X	24994	US 81	Four Mile Creek	18	Canadian	4	8300
47	0922 0369SX	24782	SH 3	S.H. 3-CREEK		Canadian	4	6000
48	0922 0480SX	24783	SH 3	Uncle John TRIB		Canadian	4	6000
49	0922 0651SX	24785	SH 3	Uncle John's Creek		Canadian	4	6000
50	6605 0059EX	25246	US 169	Caney River		Rogers	8	11900
51	6605 0090WX	25251	US 169	Caney River O'Flow		Rogers	8	11900
52	6605 0107EX	25249	US 169	Four Mile Creek-1		Rogers	8	11900
53	6606 0480WX	25254	US 169	Four Mile Creek-2		Rogers	8	11900
54	0912 0071 X	24993	US 81	U.S. 81-Up R.R. Under	19	Canadian	4	7000
55	7274 0135NX	24389	SH 67	Creek-1	20	Tulsa	8	8500
56	7274 0135SX	24390	SH 67	Creek-2		Tulsa	8	8500
57	7274 0550NX	24029	SH 67	Creek-3		Tulsa	8	8500
58	7274 0550SX	24028	SH 67	Creek-4		Tulsa	8	8500
59	4926 0403 X	24839	SH 82	Spring Creek		Mayes	8	5100
60	4926 0521 X	24836	SH 82	Snack Creek		Mayes	8	5100